

Chapter 29

Numerical Study of Stroboscopic Duffing Map

29.1 Introduction

This chapter continues the study of the Duffing equation begun in Section 1.4.3. Recall that we are interested in the behavior of the system governed by the differential equation

$$\ddot{q} + 2\beta\dot{q} + q + q^3 = -\epsilon \sin \omega\tau, \quad (29.1.1)$$

or its equivalent first-order equation pair

$$\begin{aligned}\dot{q} &= p, \\ \dot{p} &= -2\beta p - q - q^3 - \epsilon \sin \omega\tau.\end{aligned} \quad (29.1.2)$$

Because the right sides of (1.1) and (1.2) are periodic with period

$$T = 2\pi/\omega, \quad (29.1.3)$$

we were able to define stroboscopic times

$$\tau^n = nT, \quad (29.1.4)$$

and were able to reduce the study of the long-term behavior of the driven Duffing oscillator to the study of its associated stroboscopic map \mathcal{M} under repeated iteration.

As indicated in Subsection 1.4.3, the driven Duffing oscillator is expected to display an enormously rich behavior that varies widely with the parameter values β , ϵ , and ω . Consequently, even providing an overview of what can happen requires considerable work, and even then we shall be able to discuss only some of its complexity.

Our analysis will parallel that for the logistic map as done in Section 1.2.1. We will find the fixed points of \mathcal{M} for a small value of the driving strength ϵ , and track them in q, p space as the driving frequency ω is varied thereby producing a Feigenbaum/bifurcation diagram. Subsequently we will gradually increase the value of ϵ all the while observing the Feigenbaum/bifurcation diagram for \mathcal{M} as a function of ω . For simplicity, we will hold the damping parameter β at the constant value $\beta = 0.1$.¹

¹Of course, one can also make Feigenbaum diagrams in which some other parameter, say ϵ , is varied while

29.2 Review of Simple Harmonic Oscillator Behavior

But first suppose that the q^3 term in (1.1) or (1.2) were missing. Then we know how to solve the differential equation, which is just that of a driven damped simple harmonic oscillator. The solution would consist of a particular solution plus any solution of the homogeneous equation. The particular solution, call it $q_f(\tau)$, is given by the relation

$$q_f(\tau) = -A(\beta, \omega)\epsilon \sin(\omega\tau + \phi) \quad (29.2.1)$$

where

$$A(\beta, \omega) = 1/\sqrt{(1 - \omega^2)^2 + (2\beta\omega)^2} \quad (29.2.2)$$

and

$$\phi(\beta, \omega) = -\text{Arctan}[(2\beta\omega)/(1 - \omega^2)]. \quad (29.2.3)$$

Differentiating (2.1) gives the related result

$$p_f(\tau) = -\omega A(\beta, \omega)\epsilon \cos(\omega\tau + \phi). \quad (29.2.4)$$

Evidently $q_f(\tau)$ and $p_f(\tau)$ are periodic in τ with period T and therefore, as the subscript f is intended to convey, the phase-space point $\{q_f(0), p_f(0)\}$ is a *fixed* point of the stroboscopic map \mathcal{M} for the driven damped simple harmonic oscillator. Moreover, if $\beta > 0$, then all solutions of the homogeneous equation are exponentially damped as $\tau \rightarrow \infty$, and therefore $\{q_f(0), p_f(0)\}$ is a stable (and unique) attracting fixed point. We may therefore make the identification

$$\{q_\infty, p_\infty\} = \{q_f(0), p_f(0)\}. \quad (29.2.5)$$

Figures 2.1 and 2.2 display $A(\beta, \omega)$ and $\phi(\beta, \omega)$ as a function of ω for the case $\beta = .1$, and Figures 2.3 and 2.4 show q_∞ and p_∞ as functions of ω (for the case $\beta = 0.1$ and $\epsilon = .15$), and Figure 2.5 shows them both.² As expected, there is resonant behavior in the vicinity of $\omega = 1$ since the coefficient of q in (1.1) is unity.³ Also note that both q_∞ and p_∞ approach zero when ω either goes to zero or to infinity. See Exercise 2.1.

the others, including ω , are held fixed. We choose to vary ω because so doing brings resonance behavior to the fore.

²The value $\beta = .1$ for the damping coefficient corresponds to a quality factor $Q \simeq 4.95$. See Exercise 2.2.

³It was the desire for q_∞ to exhibit a resonance-like peak as a function of ω that dictated the choice (1.4.28) for ψ .

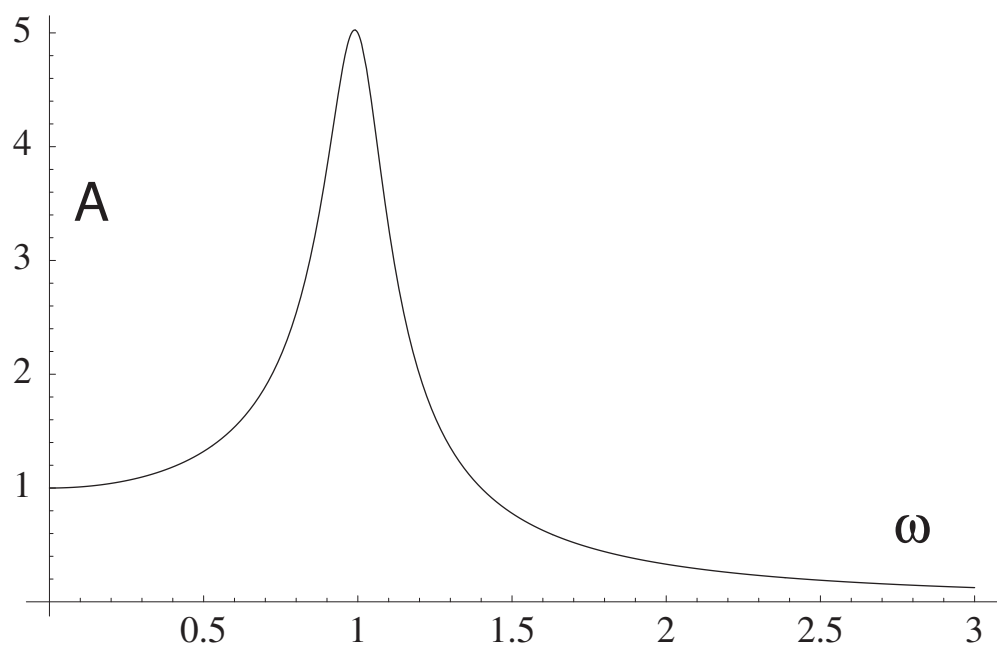


Figure 29.2.1: The quantity $A(\beta, \omega)$ as a function of ω (for the case $\beta = 0.1$).

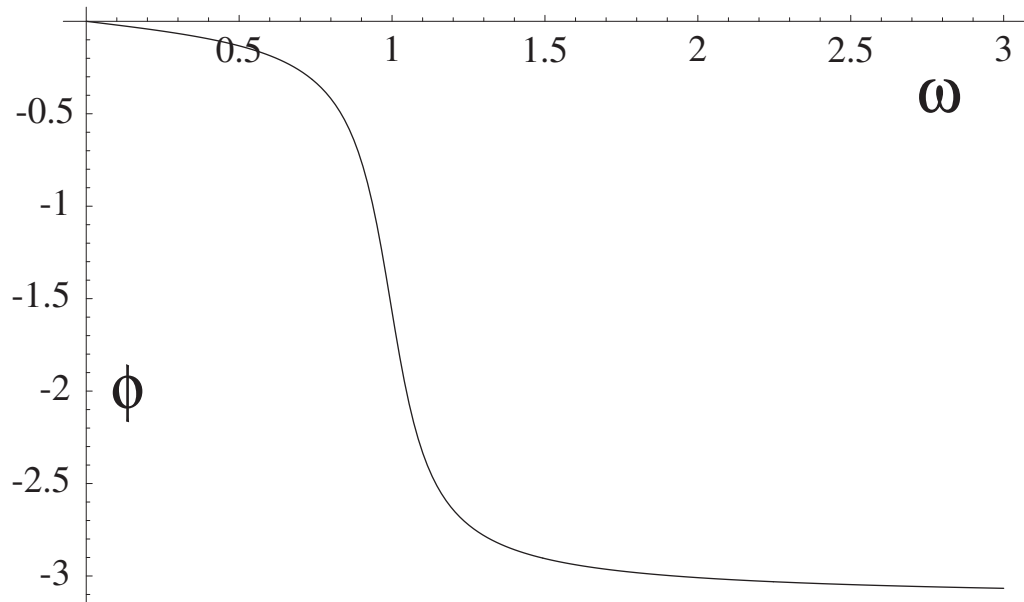


Figure 29.2.2: The quantity $\phi(\beta, \omega)$ as a function of ω (for the case $\beta = 0.1$).

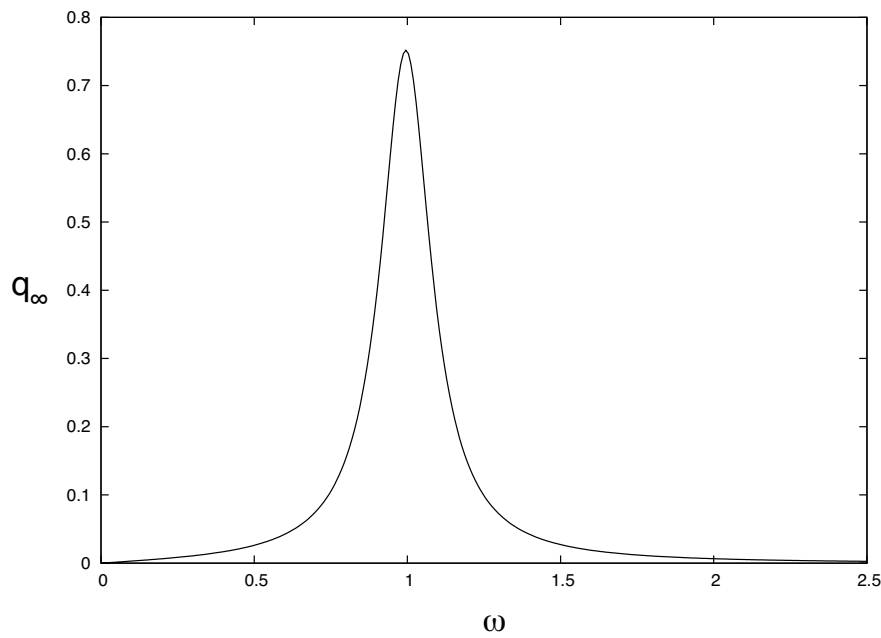


Figure 29.2.3: Feigenbaum diagram showing limiting values q_∞ as a function of ω (when $\beta = 0.1$ and $\epsilon = .15$) for the stroboscopic driven damped simple harmonic oscillator map.

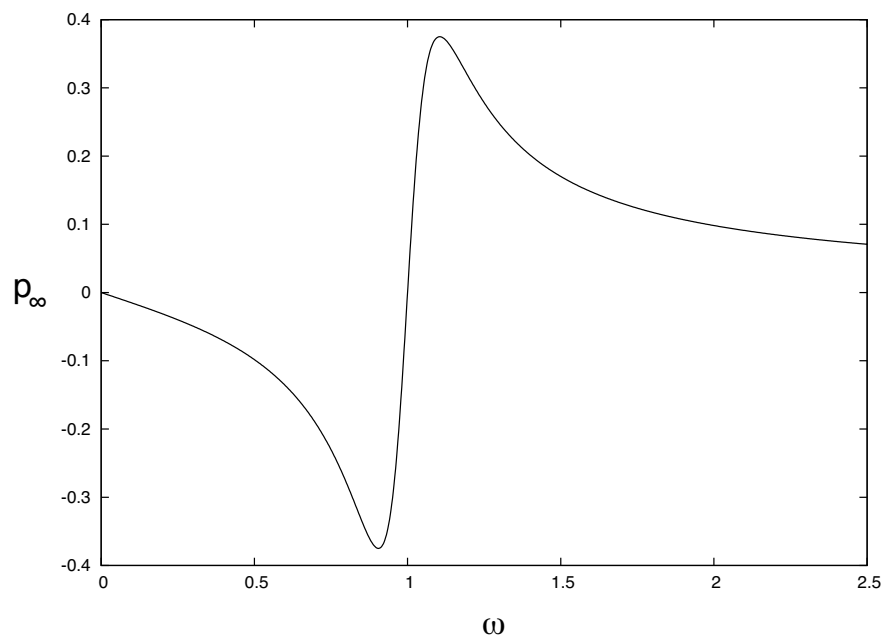


Figure 29.2.4: Feigenbaum diagram showing limiting values p_∞ as a function of ω (when $\beta = 0.1$ and $\epsilon = .15$) for the stroboscopic driven damped simple harmonic oscillator map.

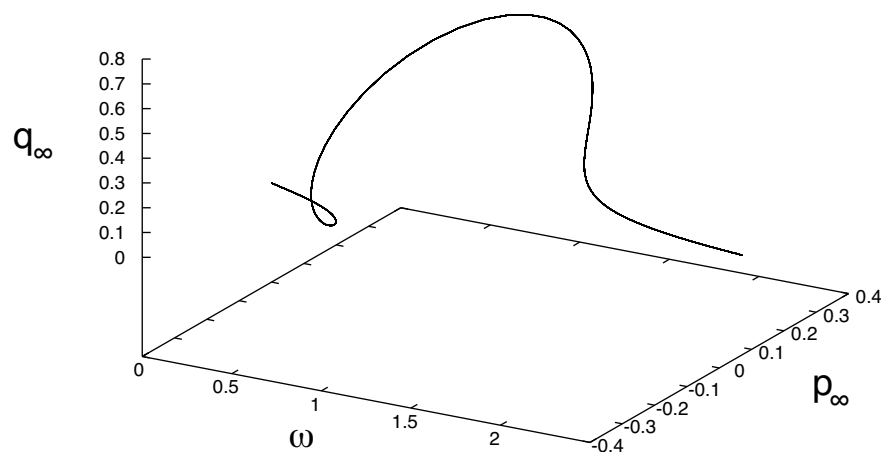


Figure 29.2.5: Feigenbaum diagram showing both limiting values q_∞ and p_∞ as a function of ω (when $\beta = 0.1$ and $\epsilon = .15$) for the stroboscopic driven damped simple harmonic oscillator map.

Exercises

29.2.1. Show, using (2.1), (2.4), and (2.5), that

$$q_\infty = -A(\beta, \omega)\epsilon \sin \phi, \quad (29.2.6)$$

$$p_\infty = -\omega A(\beta, \omega)\epsilon \cos \phi. \quad (29.2.7)$$

Show that using (2.2) and (2.3) in (2.6) and (2.7) gives the equivalent results

$$q_\infty = 2\beta\omega\epsilon/[(\omega^2 - 1)^2 + (2\beta\omega)^2], \quad (29.2.8)$$

$$p_\infty = \omega(\omega^2 - 1)\epsilon/[(\omega^2 - 1)^2 + (2\beta\omega)^2]. \quad (29.2.9)$$

Determine the behavior of q_∞ and p_∞ as ω either goes to zero or goes to infinity.

29.2.2. The *quality factor* Q of a damped harmonic oscillator is defined by the relation

$$Q = \omega_R/(2\beta) \quad (29.2.10)$$

where ω_R is the resonant frequency. For the normalization used in (1.1),

$$\omega_R^2 = 1 - 2\beta^2. \quad (29.2.11)$$

Show that $Q \simeq 4.95$ when $\beta = 0.1$.

29.3 Behavior for Small Driving when Nonlinearity is Included

If the driving strength ϵ is small enough and the damping coefficient β is large enough, then we expect $q(\tau)$ to be small, and therefore the q^3 term in (1.1) can indeed be neglected, at least in zeroth approximation. Figure 3.1 shows q_∞ as a function of ω for the case $\beta = 0.1$ and $\epsilon = .15$ when the q^3 term in (1.1) is *retained*, and Figure 3.2 shows both q_∞ and p_∞ . Now we are dealing with the stroboscopic Duffing map, and the results shown were obtained by numerical integration. Evidently these figures resemble their simple harmonic oscillator counterparts, Figures 2.3 and 2.5. In particular, there is only *one* fixed point for each value of ω and its basin is the entire q, p plane. (Consequently there are no fixed points for powers of \mathcal{M} apart from the fixed point of \mathcal{M} itself.) Note, however, the appearance of some structure near the value $\omega = 1/3$, and that the resonance peak in q_∞ near $\omega = 1$ is reduced in amplitude and slightly tipped toward the right.

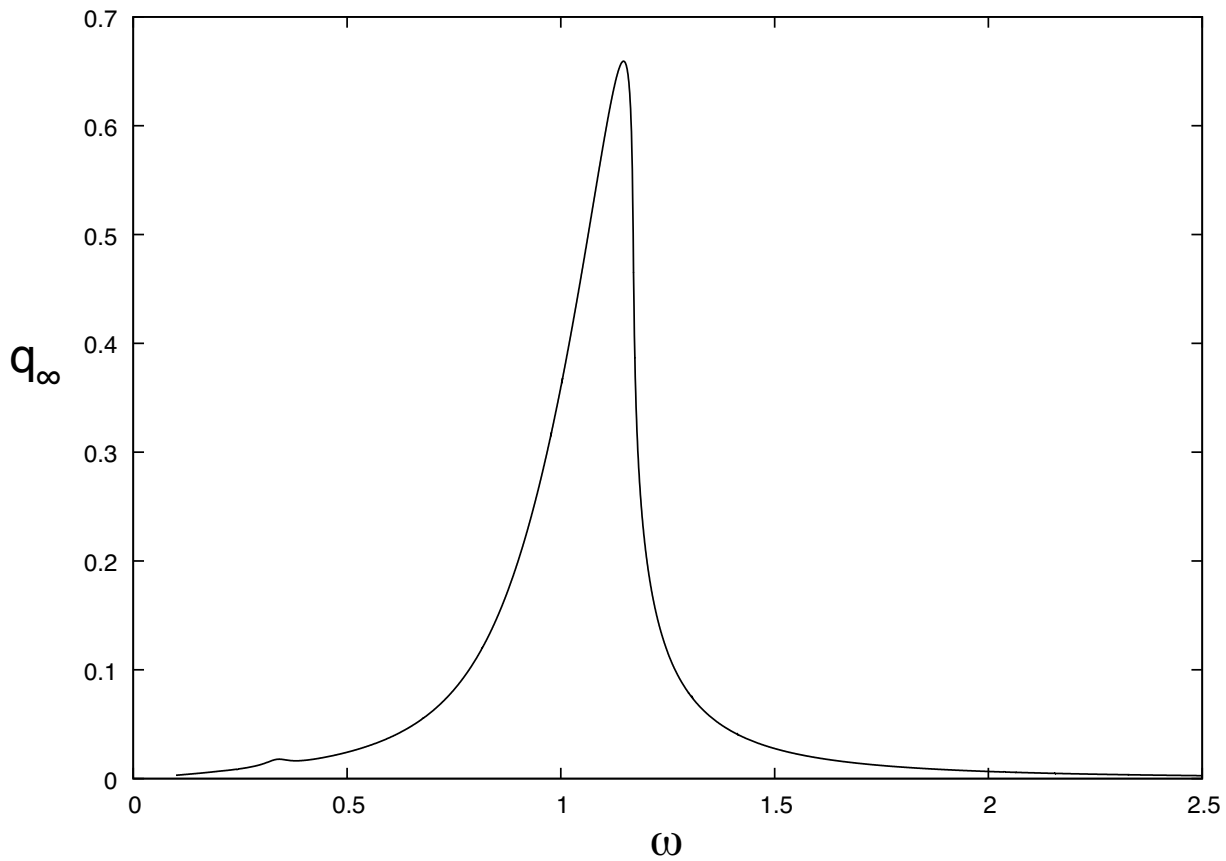


Figure 29.3.1: Feigenbaum diagram showing limiting values q_∞ as a function of ω (when $\beta = 0.1$ and $\epsilon = .15$) for the stroboscopic Duffing map.

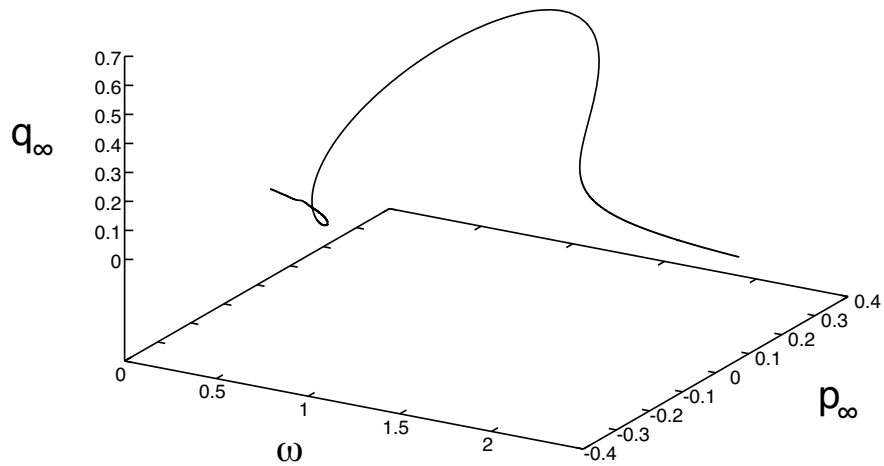


Figure 29.3.2: Feigenbaum diagram showing both limiting values q_∞ and p_∞ as a function of ω (when $\beta = 0.1$ and $\epsilon = .15$) for the stroboscopic Duffing map.

29.4 What Happens Initially When the Driving Is Increased?

29.4.1 Saddle-Node (Blue-Sky) Bifurcations

We have found the Feigenbaum diagram of the stroboscopic Duffing map for small driving strength ϵ . As promised, let us now increase ϵ to see what occurs. Figures 4.1 and 4.2 show results for the case $\epsilon = 1.5$. Evidently the height of the resonance peak has grown in response to the increased driving and has taken on a more complicated structure. And the feature originally near $\omega = 1/3$ has become a clearly defined *subresonant* peak. These peaks have also moved to larger values of ω . This is to be expected since the natural frequency of an oscillator having a hard spring increases with amplitude. Moreover, additional features now appear to the left of those already recognized.

Most striking, for $\omega \in (1.8\cdots, 2.7\cdots)$, there are *three* fixed points in place of the *single* fixed point originally present for the case of less driving. Two of these fixed points are stable and the third, whose coordinates as a function of ω are shown as a red line, is unstable. (How the unstable fixed point can be found is described in Section 29.4.) What happens is that, as ω is increased from small values, a pair of fixed points, one unstable and one stable, is ‘born’ near $\omega = 1.8\cdots$. This is sometimes called a *saddle-node* bifurcation. (The term *saddle* denotes a particular kind of unstable fixed point, and the term *node* denotes a particular kind of stable fixed point.) It is also called a *blue sky* bifurcation since these fixed points seem to appear out of nowhere, i.e. out of the blue. (They actually come out of the complex domain).⁴ Then, as ω is further increased, the unstable fixed point moves to meet and ‘annihilate’ the original fixed point at $\omega = 2.7\cdots$ in an *inverse* saddle-node (or blue sky) bifurcation thereby leaving behind only the stable fixed point born near $\omega = 1.8\cdots$. All this behavior can be understood on topological grounds. See Section 29.5.

⁴For an example of a blue sky bifurcation in the case of the one-dimensional logistic (quadratic) map, see the end of Exercise 1.2.7.

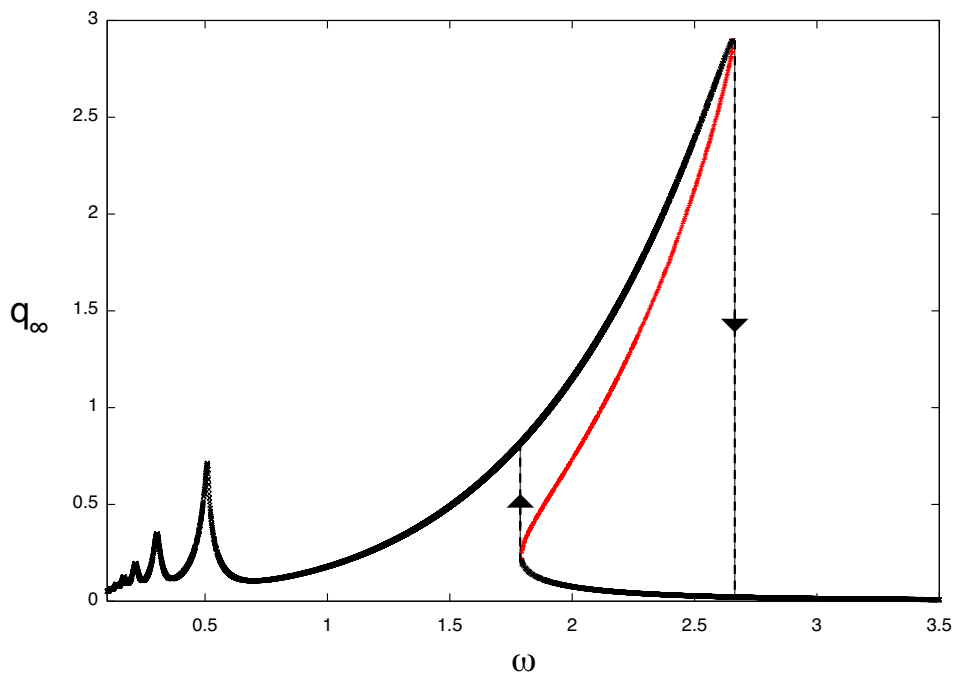


Figure 29.4.1: Feigenbaum/bifurcation diagram showing limiting values q_∞ as a function of ω (when $\beta = 0.1$ and $\epsilon = 1.5$) for the stroboscopic Duffing map. Also shown, in red, is the trail of the unstable fixed point. Finally, jumps in the steady-state amplitude are illustrated by vertical dashed lines at $\omega \simeq 1.8$ and $\omega \simeq 2.6$.

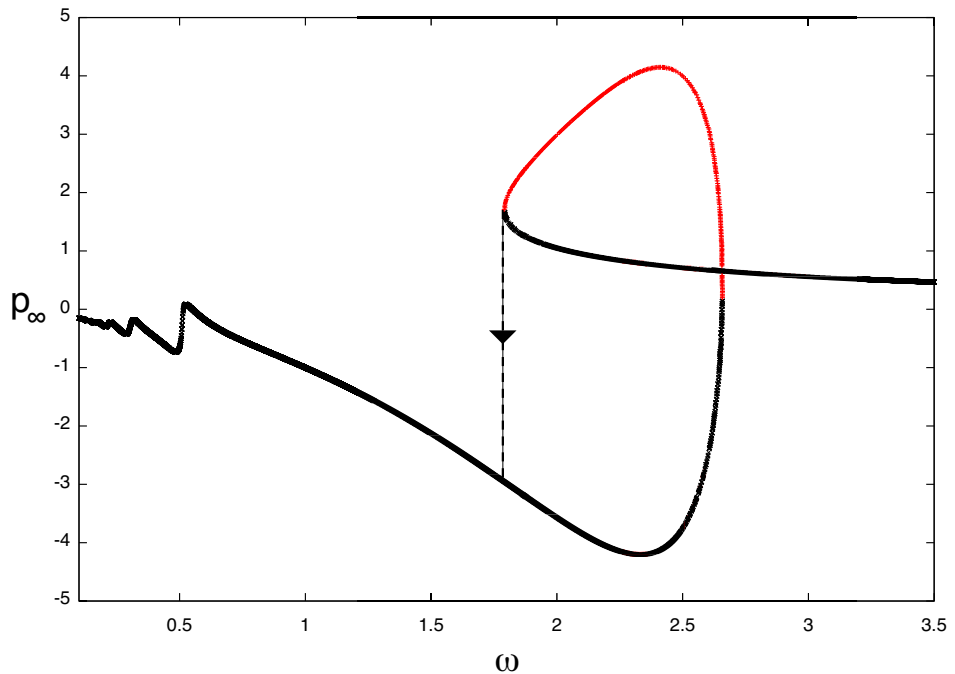


Figure 29.4.2: Feigenbaum/bifurcation diagram showing limiting values of p_∞ as a function of ω (when $\beta = 0.1$ and $\epsilon = 1.5$) for the stroboscopic Duffing map. Also shown, in red, is the trail of the unstable fixed point. Finally, a downward jump in the steady-state value p_∞ at $\omega \simeq 1.8$ is illustrated by a vertical dashed line. There is also an upward jump between the two black curves at $\omega \simeq 2.6$, but this feature is too small to be easily indicated by a second vertical dashed line.

29.4.2 Basins

Figure 4.3 shows the basins of attraction for the two stable fixed points when $\omega = 2.25$. The stable fixed points have the locations

$$w^1 = (q_\infty, p_\infty) = (0.04247237, 0.84035059) \text{ (green)} \quad (29.4.1)$$

and

$$w^2 = (q_\infty, p_\infty) = (1.68001491, -4.14472685) \text{ (red).} \quad (29.4.2)$$

The unstable fixed point has the location

$$w^3 = (q_\infty, p_\infty) = (1.32261, 3.88274). \quad (29.4.3)$$

Since these two basins together comprise the entire q, p plane, there are no other stable fixed points of \mathcal{M} . Moreover, there are no fixed points for powers of \mathcal{M} apart from the fixed points of \mathcal{M} itself. Finally, it can be shown that, unlike the complex logistic map, the basin boundaries are smooth. This is because in this case there are no homoclinic points. See Section 29.6 and Figure 29.6.8. Thus, in this parameter regime, the long-term behavior of the driven Duffing oscillator is relatively simple.⁵

What is the actual motion for the periodic orbits associated with these fixed points? Figure 4.4 shows $q(\tau)$ for the two stable fixed points, and Figure 4.5 shows $q(\tau)$ for the unstable fixed point, all for the case $\omega = 2.25$. At this point one can make two interesting observations.

29.4.3 Symmetry

The first observation is that if $q(\tau)$ is a solution (periodic or otherwise) to Duffing's equation, then so is $\bar{q}(\tau)$ with

$$\bar{q}(\tau) = -q(\tau - \pi/\omega). \quad (29.4.4)$$

Note that, in view of (1.3), there is the relation

$$\pi/\omega = T/2 \quad (29.4.5)$$

so that (4.4) can also be written in the form

$$\bar{q}(\tau) = -q(\tau - T/2). \quad (29.4.6)$$

This property is an example of what is sometimes called *equivariance*, and occurs in this case because the left side of (1.1) is odd in q and does not explicitly contain the time. See Exercise 4.1. Thus, given a solution q of Duffing's equation, use of (4.6) produces a related solution \bar{q} . In principle this solution may be different, but it could also be the same as the original one. Inspection of Figures 4.4 and 4.5 reveals that

$$\bar{q}(\tau) = q(\tau) \quad (29.4.7)$$

⁵We remark that there would be no attractors, and consequently no basins, in the zero damping limit $\beta \rightarrow 0$, for then the system would be Hamiltonian, and we have learned in Subsections 3.4 and 6.4 that Hamiltonian systems have neither attractors or repellers. That is one reason why the long-term behavior of most Hamiltonian systems is so complicated.

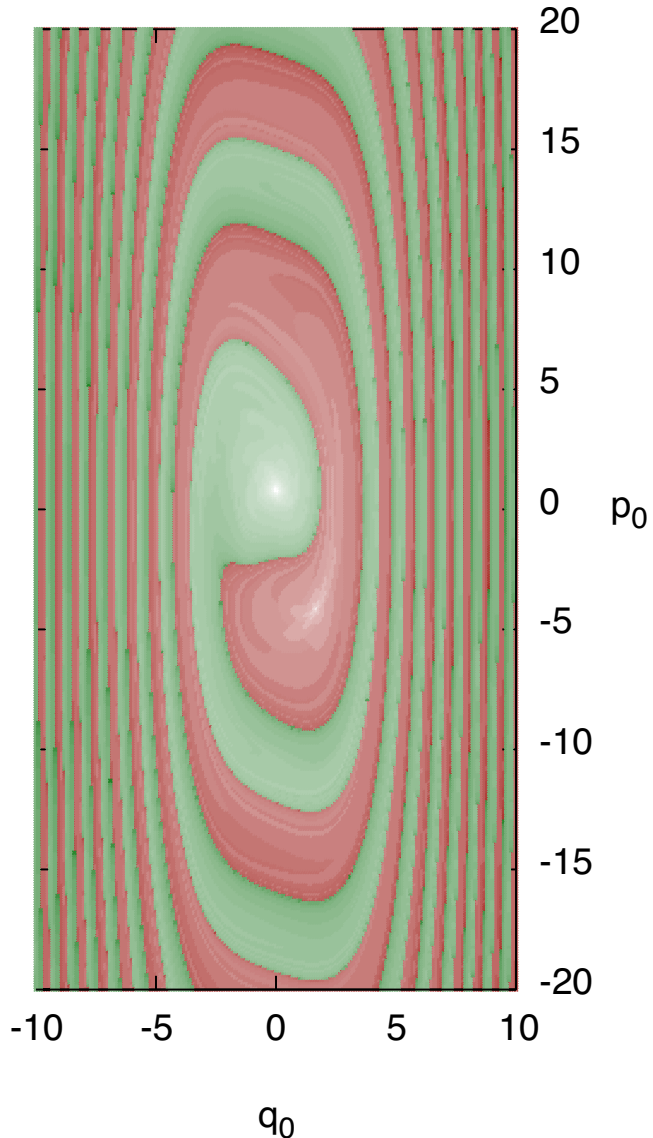


Figure 29.4.3: Basins of attraction for the two stable fixed points (when $\omega = 2.25$, $\beta = 0.1$, and $\epsilon = 1.5$) for the stroboscopic Duffing map. Green points are in the basin of the attracting fixed point w^1 and red points are in the basin of the attracting fixed point w^2 . There is also an unstable fixed point w^3 . See Figures 29.6.7 and 29.6.8.

for all three periodic orbits shown. Therefore in this case each solution is sent into itself under the ‘barring’ operation. It can be verified that the same is true for all the periodic solutions associated with all the fixed points found so far.

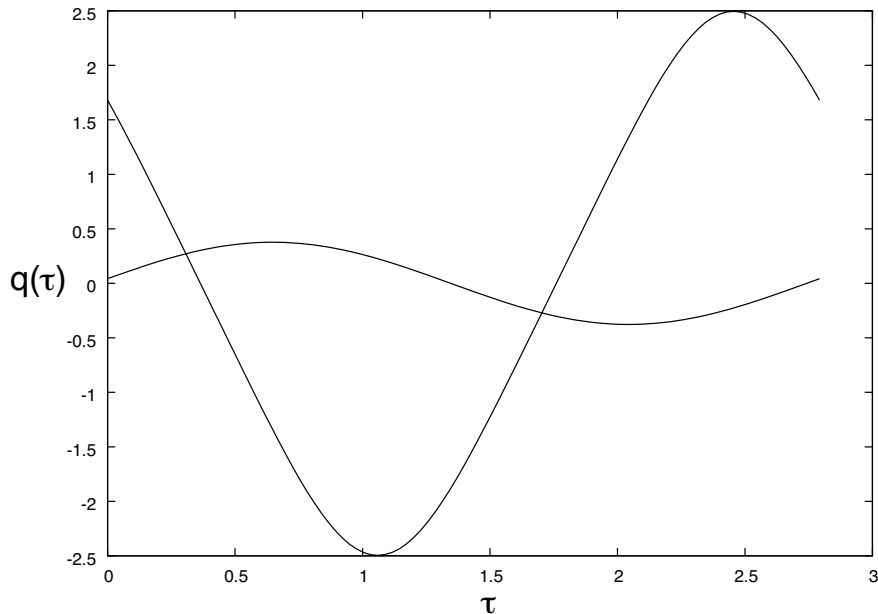


Figure 29.4.4: Stable periodic orbits $q(\tau)$ (when $\omega = 2.25$, $\beta = 0.1$, and $\epsilon = 1.5$) for the Duffing equation.

29.4.4 Amplitude Jumps

The second observation is that the two stable periodic orbits shown in Figure 4.4 have *different* amplitudes. With reference to Figures 4.1 and 4.2, suppose that $\omega \simeq 1.5$ and that the Duffing oscillator has settled down to the periodic orbit associated with the attracting fixed point q_∞, p_∞ . (For this value of ω there is only one fixed point, and it is attracting.) Next imagine slowly increasing ω (*slowly* means in a time large compared to the time required to settle down to the attracting periodic orbit). Then the Duffing oscillator will essentially remain on the periodic orbit associated with the value of q_∞ shown as the upper curve in Figure 4.1. This will continue to be the case until ω reaches the value $\omega \simeq 2.6$, at which value the stable fixed point merges with the unstable fixed point and they mutually annihilate. What has happened is that the basin of attraction of this stable fixed point has shrunk to zero. When this occurs, the oscillator orbit finds itself in the basin of the other remaining stable fixed point and is rapidly attracted to the periodic orbit associated with that stable fixed point. Moreover, as Figure 4.1 suggests and Figure 4.4 confirms, the amplitude of oscillation associated with this new periodic orbit is considerably less than that associated with the old. Thus, the Duffing oscillator exhibits an *amplitude jump* (to an appreciably *lower* value) as ω is increased beyond $\omega \simeq 2.6$. This amplitude jump is illustrated by the vertical dashed lines at $\omega \simeq 2.6$ in Figures 4.1 and 4.2.

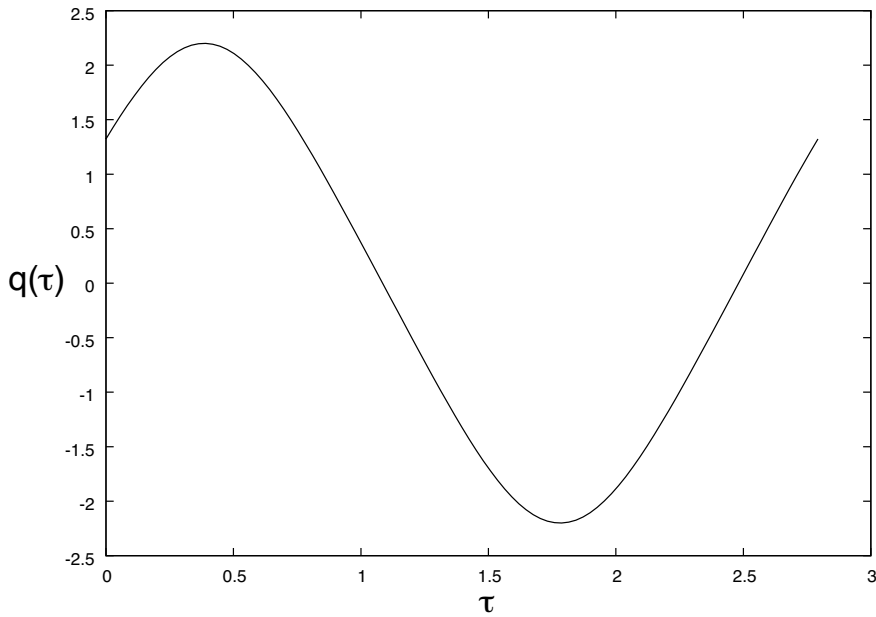


Figure 29.4.5: Unstable periodic orbit $q(\tau)$ (when $\omega = 2.25$, $\beta = 0.1$, and $\epsilon = 1.5$) for the Duffing equation.

29.4.5 Hysteresis

Next suppose that $\omega > 2.6$, say $\omega \simeq 3$, and that the Duffing oscillator has settled down to the periodic orbit associated with the attracting fixed point q_∞, p_∞ . (For this value of ω there is again only one fixed point, and it is attracting.) Now slowly decrease ω . Then the Duffing oscillator will essentially remain on the periodic orbit associated with the value of q_∞ shown as the lower curve in Figure 4.1. This will continue to be the case until ω reaches the value $\omega \simeq 1.8$, at which value the stable fixed point in question merges with the unstable fixed point and they mutually annihilate. What has happened is that the basin of attraction of this stable fixed point has now shrunk to zero. When this occurs, the oscillator orbit finds itself in the basin of the other remaining stable fixed point and is rapidly attracted to the periodic orbit associated with that stable fixed point. Now the amplitude of oscillation will jump to a *larger* value. This amplitude jump is also illustrated by vertical dashed lines at $\omega \simeq 1.8$ in Figures 4.1 and 4.2. Note that the ω values for the two amplitude jumps are different. Thus, the steady-state amplitude of the Duffing oscillator exhibits *hysteresis* as ω is slowly varied back and forth over the range in which saddle-node bifurcations occur.

Exercises

- 29.4.1.** Show that the left side of (1.1) changes sign under the replacement of q by $-q$. Show that the right side of (1.1) changes sign under the replacement of τ by $(\tau - \pi/\omega)$. Verify that if $q(\tau)$ is a solution to Duffing's equation, then so is $\bar{q}(\tau)$ as given by (4.4) or (4.6). Let $\bar{\bar{q}}$ denote the result of applying the barring operation to \bar{q} . Show that if q is a solution associated with a fixed point of \mathcal{M} , and therefore is a periodic solution with period

T , then $\bar{\bar{q}} = q$. Verify that the harmonic oscillator solution (2.1) satisfies (4.7).

29.5 Pitchfork Bifurcations and Symmetry

Let us continue to increase ϵ . Figure 5.1 shows that a qualitatively new feature appears when ϵ is near 2.2: a *bubble* is formed *between* the major resonant peak (the one that has saddle-node bifurcated) and the subresonant peak immediately to its left. To explore the nature of this bubble, let us make ϵ still larger, which, we anticipate, will result in the bubble becoming larger. Figures 5.2 and 5.3 show Feigenbaum diagrams in the case $\epsilon = 5.5$. Now the major resonant peak and the subresonant peak have moved to larger ω values. Correspondingly, the bubble between them has also moved to larger ω values. Moreover, it is larger, yet another smaller bubble has formed, and the subresonant peak between them has also undergone a saddle-node bifurcation. For future use, we will call the major resonant peak the *first* or *leading* saddle-node bifurcation, and we will call the subresonant peak between the two bubbles the *second* saddle-node bifurcation, etc. Also, we will call the bubble just to the left of the first saddle-node bifurcation the *first* or *leading* bubble, and the next bubble will be called the *second* bubble, etc.

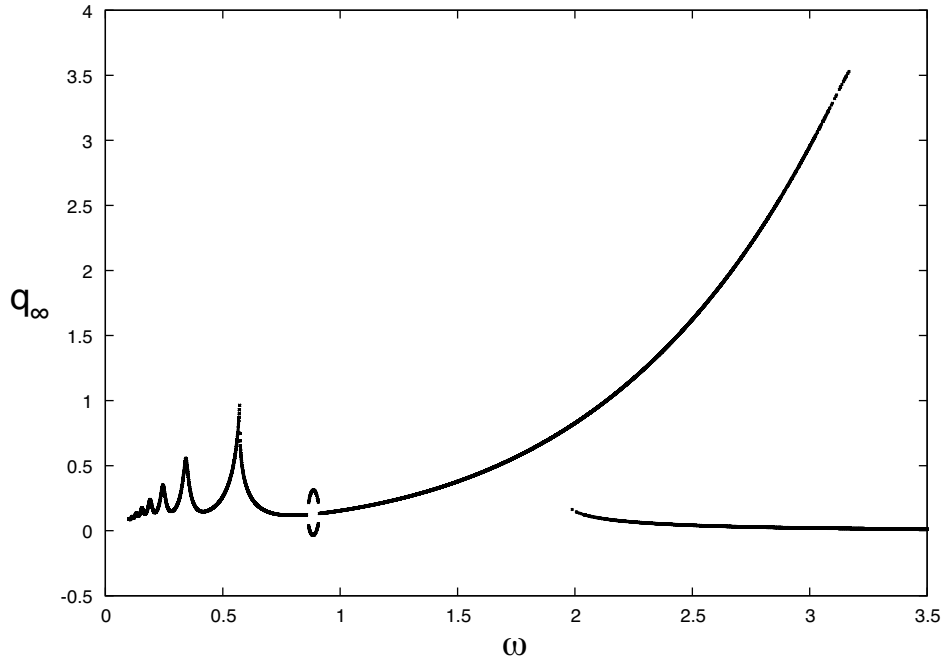


Figure 29.5.1: Feigenbaum diagram showing limiting values q_∞ as a function of ω (when $\beta = 0.1$ and $\epsilon = 2.2$) for the stroboscopic Duffing map. It displays that a bubble has now formed at $\omega \approx .8$.

Figure 5.4 shows the larger (leading) bubble in Figure 5.2 in more detail and with the addition of red lines indicating the trails of unstable fixed points. It reveals that the bubble describes the *simultaneous* bifurcation of a single fixed point into three fixed points. Two of these fixed points are stable and the third, whose q coordinate as a function of ω is shown as

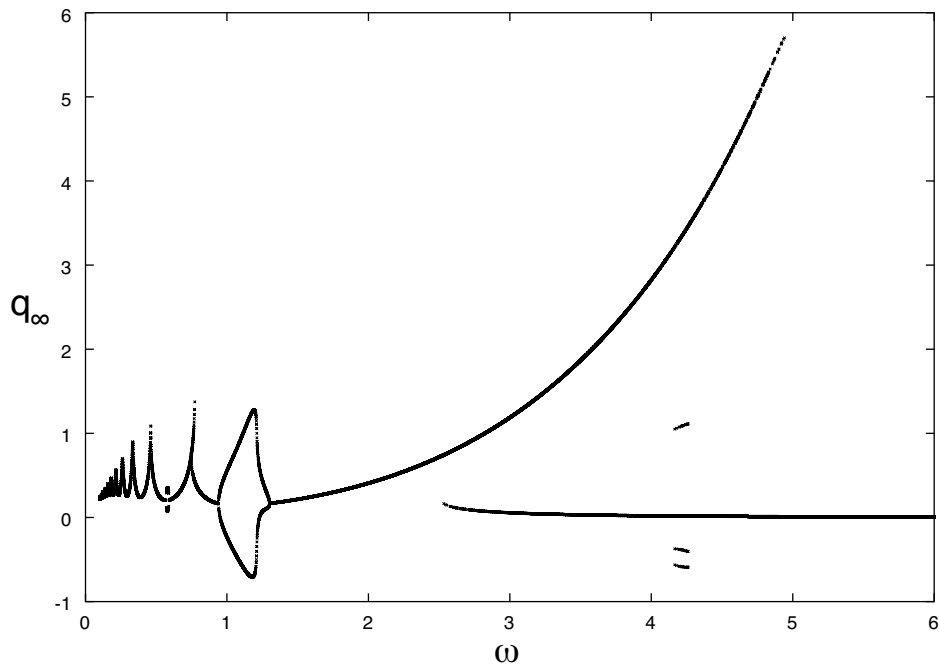


Figure 29.5.2: Feigenbaum diagram showing limiting values q_∞ as a function of ω (when $\beta = 0.1$ and $\epsilon = 5.5$) for the stroboscopic Duffing map. The first bubble has grown, a second smaller bubble has formed to its left, and the sub-resonant peak between them has saddle-node bifurcated to become the second saddle-node bifurcation.

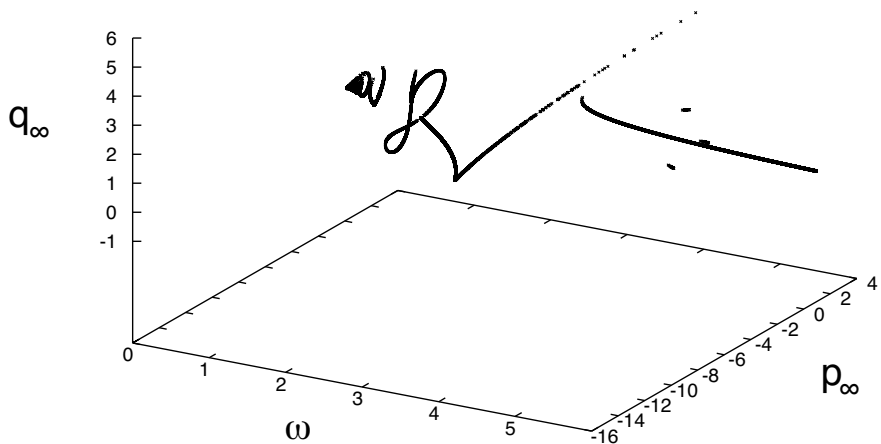


Figure 29.5.3: Feigenbaum diagram showing both limiting values q_∞ and p_∞ as a function of ω (when $\beta = 0.1$ and $\epsilon = 5.5$) for the stroboscopic Duffing map.

a red line, is unstable. What happens is that, as ω is increased, a *single* stable fixed point becomes a *triplet* of fixed points, two of which are stable and one of which is unstable. This is called a *pitchfork* bifurcation. Then, as ω is further increased, these three fixed points again merge, in an inverse pitchfork bifurcation, to form what is again a single stable fixed point. This behavior can also be understood on topological grounds. Again see Section 29.5.

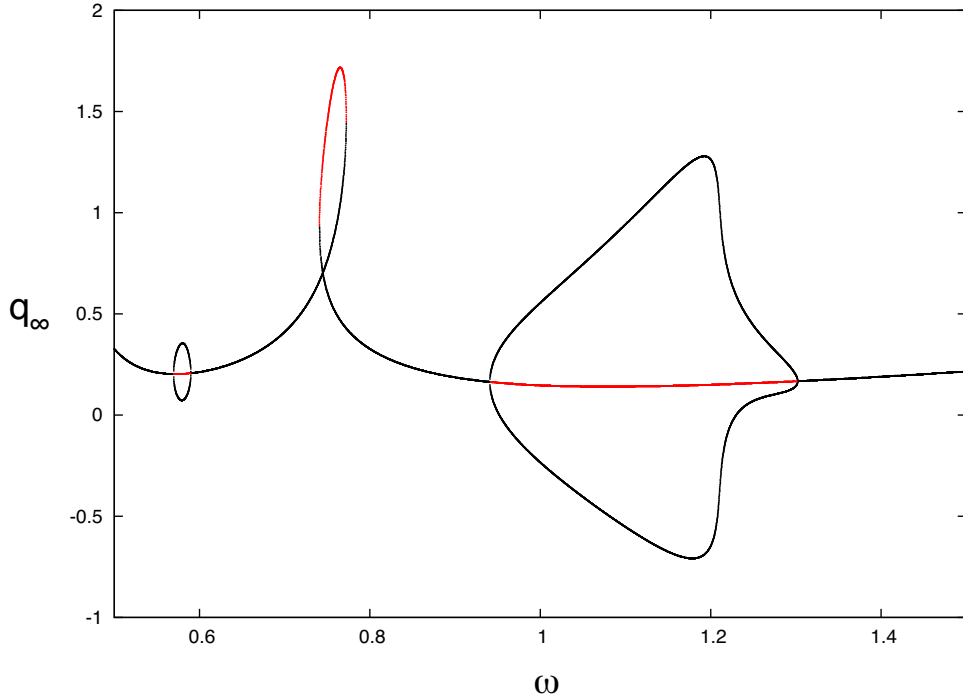


Figure 29.5.4: An enlargement of Figure 5.2 with the addition of red lines indicating the trails of unstable fixed points.

As a side comment, we remark that a pitchfork bifurcation could better be called a pitchfork *trifurcation*. Unlike a saddle-node bifurcation, in this case all three fixed points appear where once there was only one. True pitchfork bifurcations are rare, and only occur in the presence of symmetry, in this case the equivariance symmetry described earlier. However, it can happen, particularly in the case of near symmetry, that a saddle-node bifurcation occurs very close to another stable fixed point so that from a distance what appears to be happening is a pitchfork bifurcation. As an example of near symmetry, the left side of (1.1) could be modified (perturbed) to contain an additional term of the form δq^2 where δ is small. Figure 5.5 illustrates how Figure 5.4 is modified when the term $0.02q^2$ is added to the left side of (1.1). Evidently the pitchfork bifurcation becomes a saddle-node bifurcation. A pair of fixed points, one stable and one unstable, is born in the vicinity of $\omega = 1$, and they move as ω is increased. However, unlike the case of Figure 4.1, they then annihilate *each other* near $\omega = 1.3$ rather than the unstable fixed point moving up to the other fixed point so that this pair is mutually annihilated. Note also that the perturbation destroys the small bubble that was near $\omega = .6$ (which was also a pitchfork bifurcation before the perturbation was introduced).

To continue with the case of the pitchfork bifurcation, and as we did in the case of a

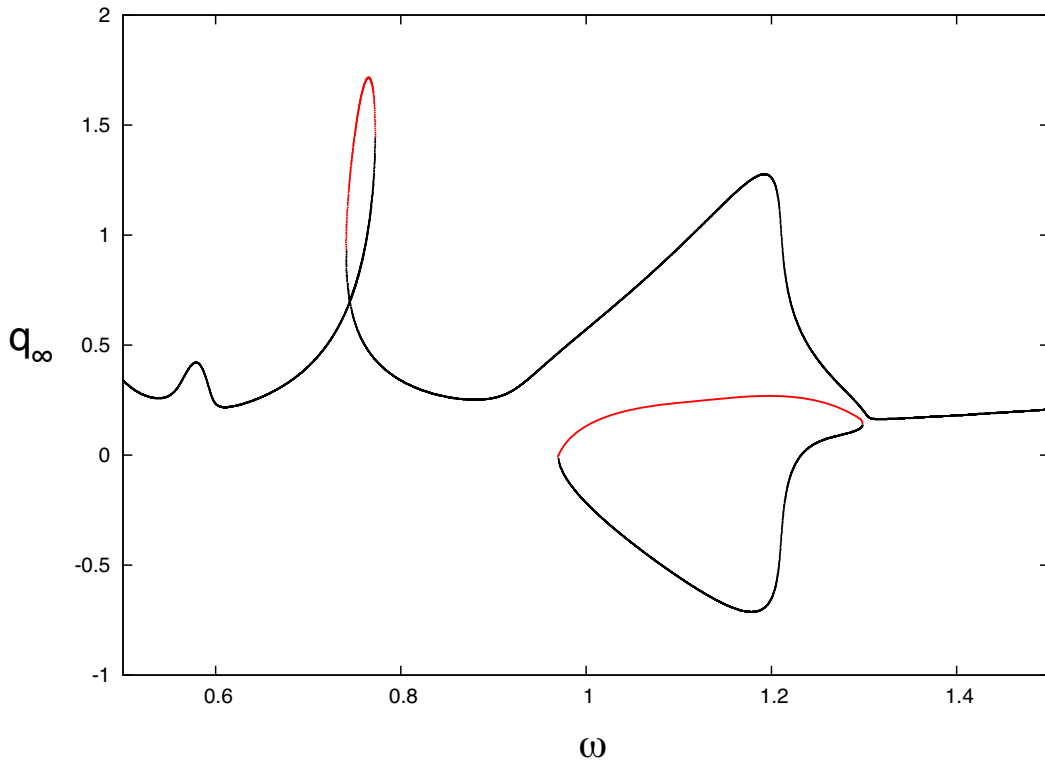


Figure 29.5.5: Transformation of a pitchfork bifurcation into a saddle-node bifurcation due to the inclusion of the symmetry breaking perturbation $0.02q^2$. Also shown as red lines are the trails of unstable fixed points. Note, however, that the stable-unstable pair of fixed points born at $\omega \approx 1$ self annihilates at $\omega \approx 1.3$ rather than the unstable fixed point annihilating the other stable fixed point as happens in Figure 4.1.

saddle-node bifurcation, let us plot the three periodic orbits associated with the three fixed points. Figure 5.6 displays $q(\tau)$ for the two stable fixed points, and Figure 5.7 displays $q(\tau)$ for the unstable fixed point, all for the case $\omega = 1.1$. The stable fixed points have the locations

$$(q_\infty, p_\infty) = (0.942055303, -0.792682910) \quad (29.5.1)$$

and

$$(q_\infty, p_\infty) = (-0.55292184, -1.72277791). \quad (29.5.2)$$

The unstable fixed point has the location

$$(q_\infty, p_\infty) = (0.140706, -1.05507). \quad (29.5.3)$$

In this case inspection shows that the unstable periodic orbit is sent into itself under the barring operation, as before. However, unlike the saddle-node case, the two stable orbits are *interchanged* under the barring operation.⁶ Also, since the amplitudes of the two stable periodic oscillations are the same as a result of their being interchanged under the barring operation (see Figure 5.6), there are no amplitude jumps associated with pitchfork bifurcations.

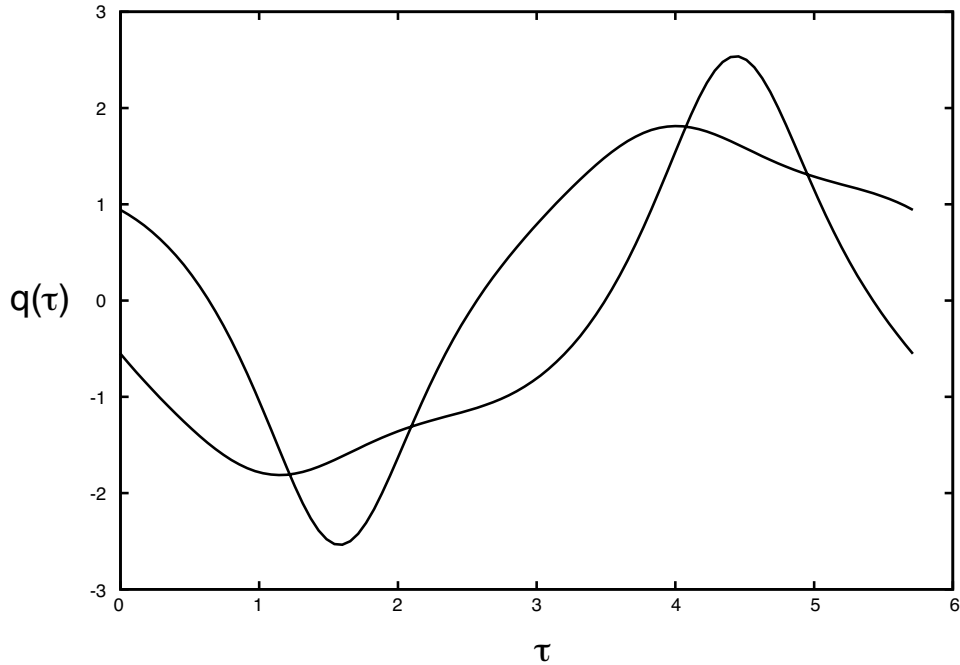


Figure 29.5.6: Stable periodic orbits $q(\tau)$ (when $\omega = 1.1$, $\beta = 0.1$, and $\epsilon = 5.5$) for the Duffing equation.

⁶The change in the nature of periodic Duffing orbits at a pitchfork bifurcation is sometimes described as *dynamical spontaneous symmetry breaking*. For small ϵ values and all ω values, all periodic orbits have the symmetry property of being invariant (sent into themselves) under the barring operation. For larger ϵ values, as ω is varied, some periodic orbits appear that no longer have this symmetry, even though the underlying equations of motion retain the same symmetry for all values of ϵ and ω .

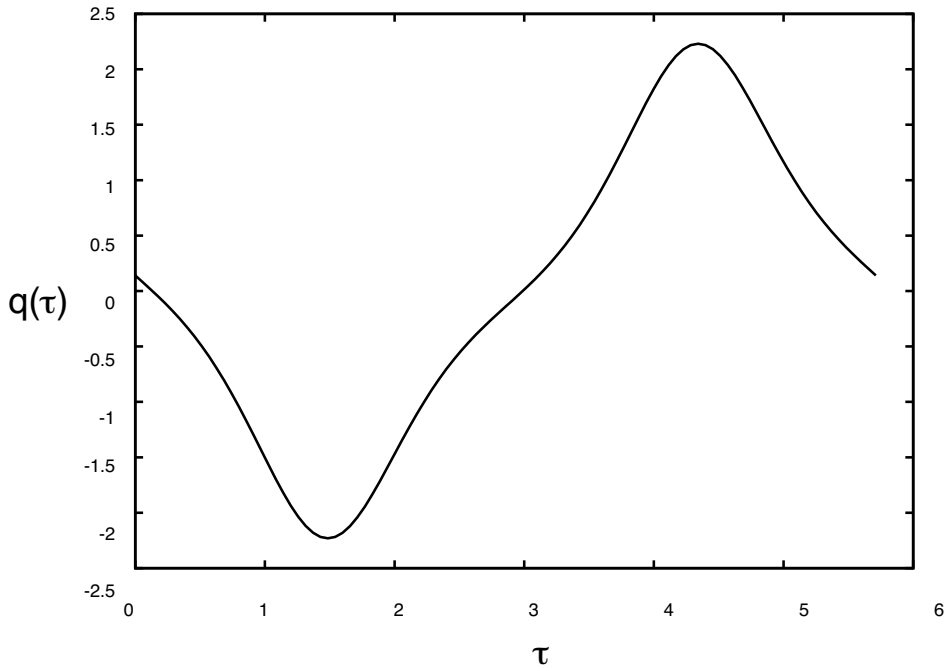


Figure 29.5.7: Unstable periodic orbit $q(\tau)$ (when $\omega = 1.1$, $\beta = 0.1$, and $\epsilon = 5.5$) for the Duffing equation.

29.6 Period Tripling Bifurcations and Fractal Basin Boundaries

Close examination of Figures 5.2 and 5.3 shows that something also happens in the vicinity of $\omega = 4.15$: Three attracting fixed points of \mathcal{M}^3 appear and then again vanish as ω is varied. Although these points are fixed points of \mathcal{M}^3 , they are not fixed points of \mathcal{M} , and hence are *period-three* fixed points of \mathcal{M} . They correspond to solutions that do not have period T , but rather are periodic with period $3T$. Solutions that are not periodic with the drive period T , but are periodic with a period that is some integer multiple of T , are said to be *subharmonic*.⁷

Figure 6.1 shows an enlargement of that portion of Figure 5.2 where period tripling occurs. The period-three fixed points are shown in green and the period-one fixed points, both stable and unstable and unstable, are shown in red. What happens is that \mathcal{M}^3 exhibits saddle-node (blue-sky) bifurcations so that \mathcal{M}^3 fixed points are born (and subsequently annihilate) in pairs. Three of each pair, those that are attracting, are shown in Figures 5.2 and 5.3. Figure 6.1 shows the period-one fixed points in red (two stable and one unstable) and the period-three fixed points in green. Inspection of the green features suggests that there are six fixed points of \mathcal{M}^3 that occur as stable-unstable pairs. Figures 6.2 through

⁷If a periodic solution has period nT , it has fundamental frequency ω/n . Correspondingly, such a solution is called $1/n$ subharmonic. For the case being discussed here, $n = 3$. It is sometimes stated in the literature that for the driven Duffing equation there is no subharmonic corresponding to the case $n = 2$, which would be the case of period *doubling*. However, we will eventually see that, for sufficiently strong driving, period doubling does occur.

6.4 confirm this analysis. They show each pair of saddle and node fixed points of \mathcal{M}^3 as functions of ω .

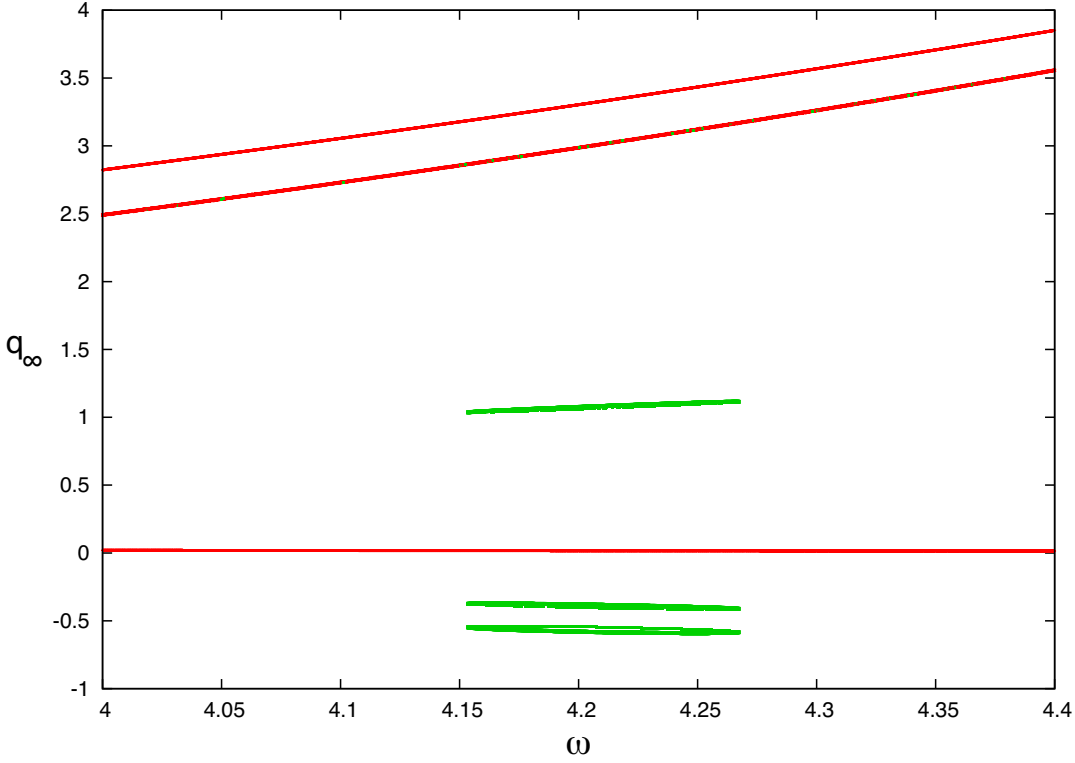


Figure 29.6.1: An enlargement of Figure 5.2 showing, for \mathcal{M} , the period-one fixed points in red (two stable and one unstable) and the stable-unstable pairs of period-three fixed points in green.

What can be said about the basin structure of \mathcal{M} and \mathcal{M}^3 in this case? Let us set

$$\omega = 4.21, \quad (29.6.1)$$

which is a convenient value roughly midway between the birth and annihilation values of ω for the period-three fixed points in Figures 6.1 through 6.4. Numerical study shows that for this value of ω there are the following attracting fixed points:

$$w^1 = (0.01666814, 1.38706838) \text{ (white)}, \quad (29.6.2)$$

$$w^2 = (3.32944854, -15.41028862) \text{ (blue)}; \quad (29.6.3)$$

$$z^1 = (1.08279489, 1.40756189) \text{ (red)}, \quad (29.6.4)$$

$$z^2 = \mathcal{M}z^1 = (-0.58378622, 0.30474951) \text{ (green)}, \quad (29.6.5)$$

$$z^3 = \mathcal{M}z^2 = (-0.38267261, 2.82716098) \text{ (yellow)}. \quad (29.6.6)$$

The points w^1 and w^2 are the attracting fixed points of \mathcal{M} . Of course, they will also be attracting fixed points of \mathcal{M}^3 . The points z^1, z^2, z^3 are the attracting fixed points of \mathcal{M}^3 ,

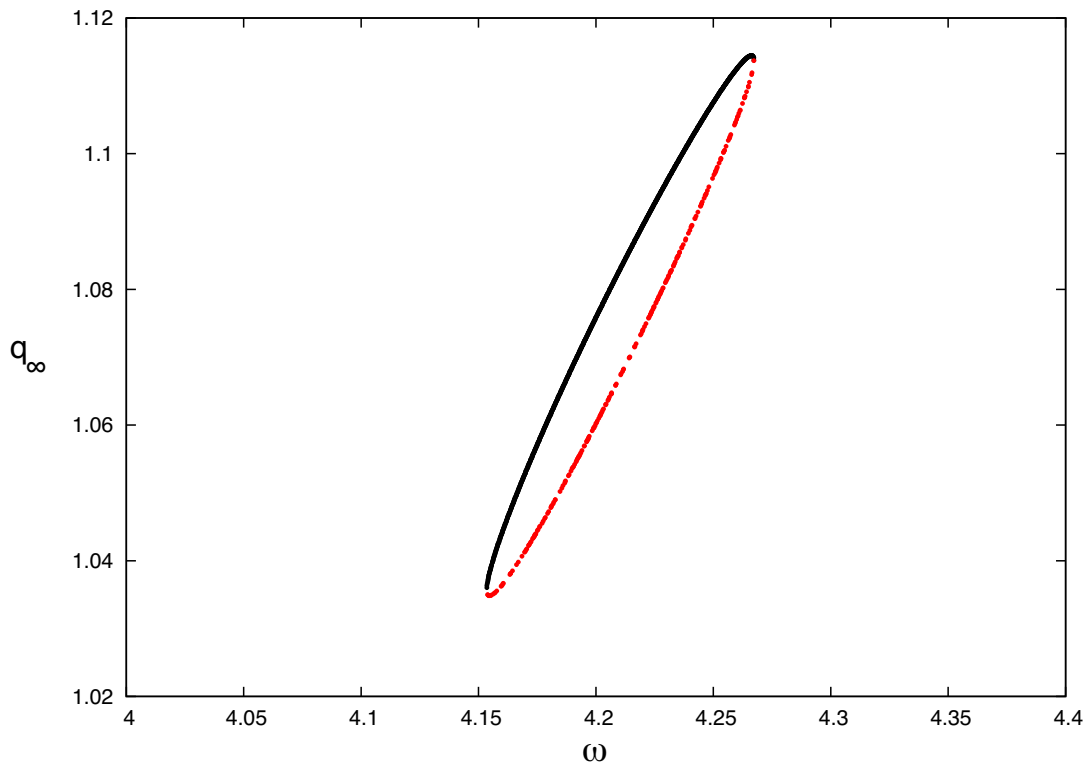


Figure 29.6.2: A blue-sky bifurcation that produces, and then subsequently destroys, a pair of stable (black) and unstable (red) period-three fixed points. These points correspond to the upper green feature shown in Figure 6.1.

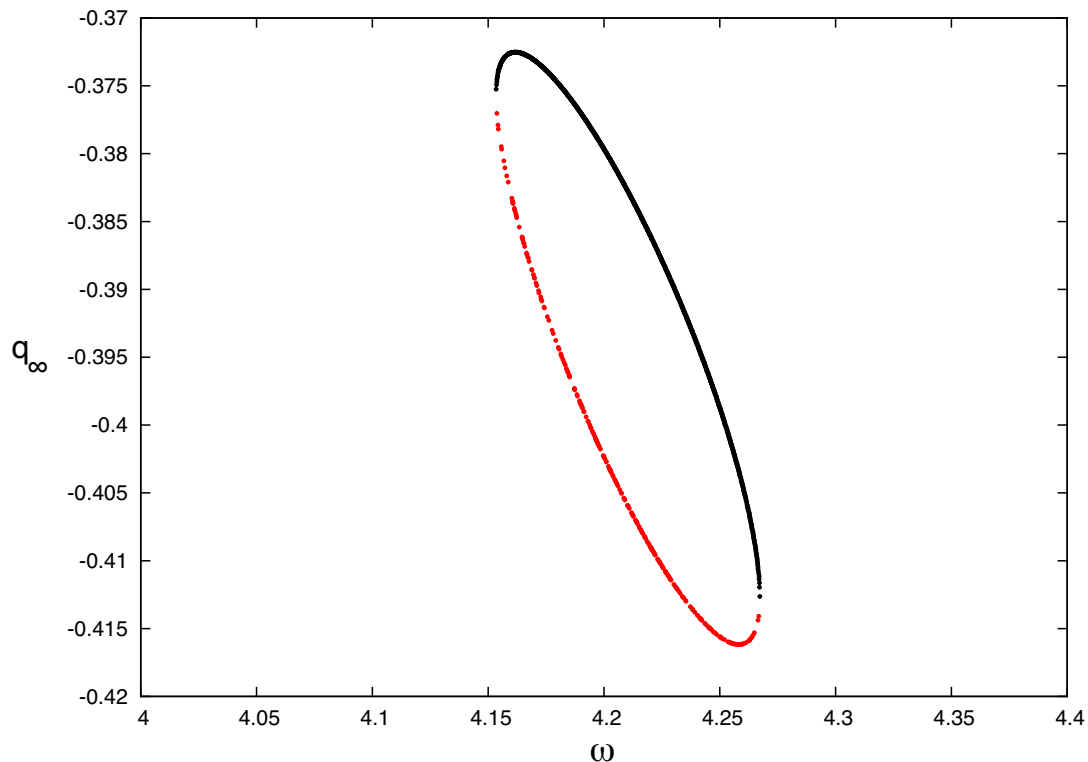


Figure 29.6.3: A blue-sky bifurcation that produces, and then subsequently destroys, a pair of stable (black) and unstable (red) period-three fixed points. These points correspond to the center green feature shown in Figure 6.1.

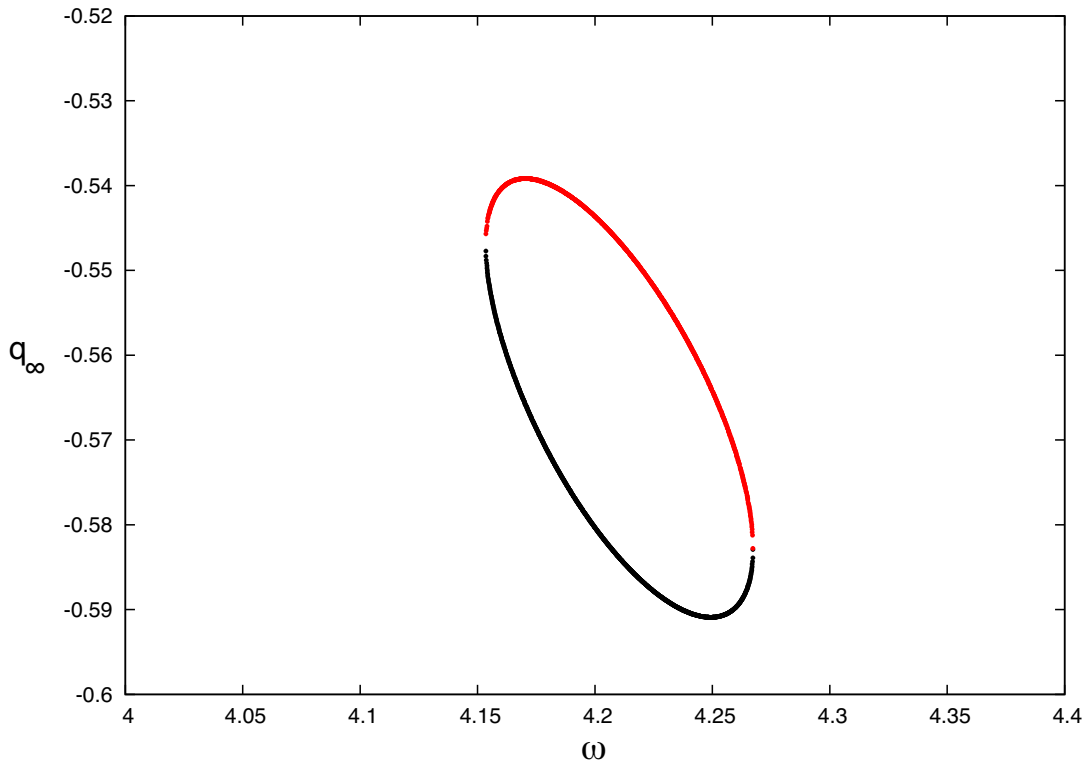


Figure 29.6.4: A blue-sky bifurcation that produces, and then subsequently destroys, a pair of stable (black) and unstable (red) period-three fixed points. These points correspond to the bottom green feature shown in Figure 6.1.

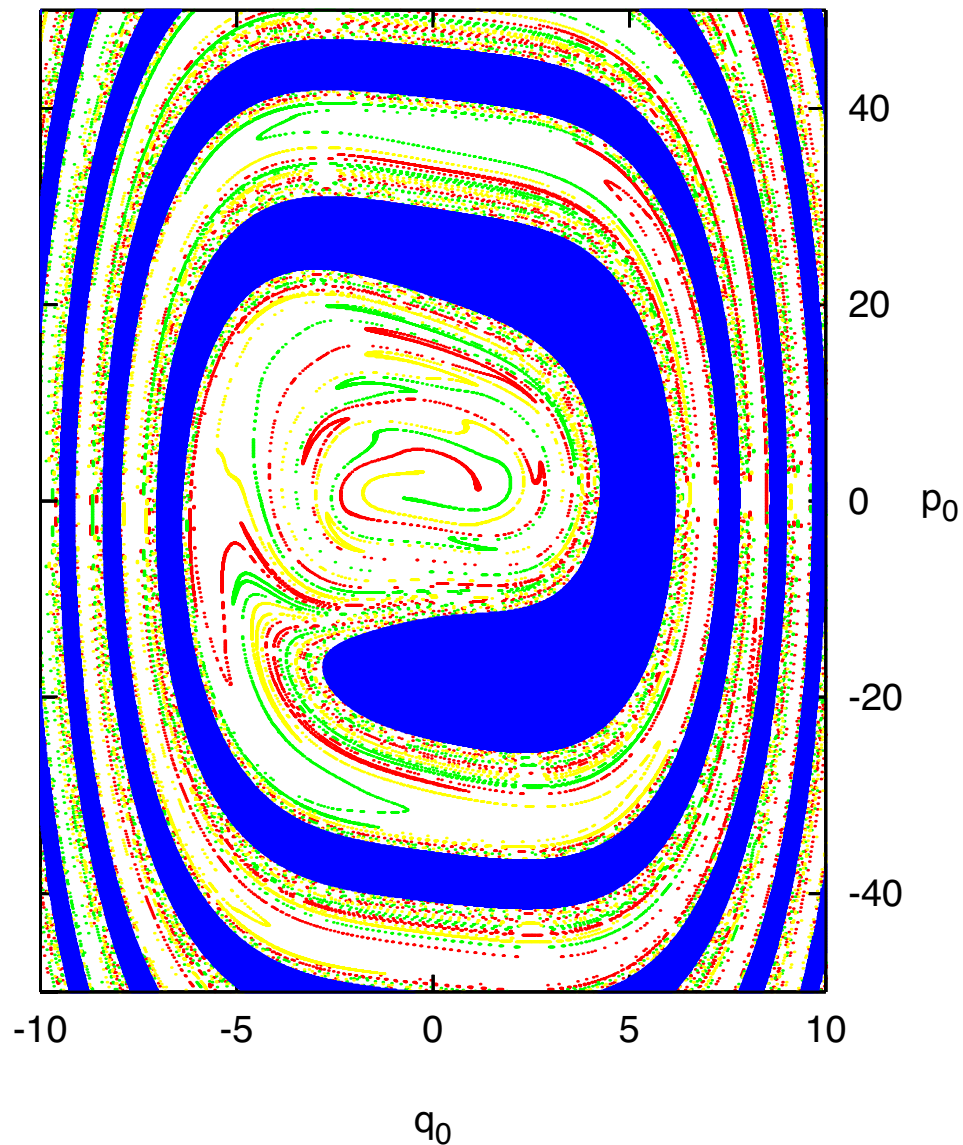


Figure 29.6.5: Basins, using the map \mathcal{M}^3 and with $\omega = 4.21$, for the period-one attracting fixed points w^1 (white) and w^2 (blue), and the period-three attracting fixed points z^1 (red), z^2 (green), and z^3 (yellow).

and hence attracting period-three fixed points of \mathcal{M} . Figure 6.5 displays, using the map \mathcal{M}^3 , the basins for all these attracting fixed points.

When viewed from a distance, the basins of w^1 and w^2 in Figure 6.5 look much like those in Figure 4.3. However, closer inspection of the white basin, that of w^1 , reveals that it contains within it the basins of the period-three fixed points z^1 , z^2 , and z^3 . Moreover, the basins of the period-three fixed points consist of principal components (which contain the period-three fixed points z^1 , z^2 , and z^3 themselves) plus what appear to be an infinite number of disconnected pieces. (Recall that all white points are in the basin of w^1 .) Finally, the pieces of the period-three basins crowd ever more closely together (but still separated by ever smaller white areas) in the vicinity of the boundary of the w^2 (blue) basin so that this basin-boundary structure becomes fractal. These features are seen even more clearly in Figure 6.6, which is an enlargement (with different q , p scales) of Figure 6.5 in the vicinity of the points w^1 , z^1 , z^2 , and z^3 . In this figure the fixed points w^1 and z^1 , z^2 , and z^3 themselves are shown as small black dots. Because the basin-boundary structure is fractal, the final fate of an orbit launched in the vicinity of the basin boundary (which of the five attracting fixed points w^1 , w^2 , z^1 , z^2 , and z^3 it eventually approaches) depends very sensitively on the initial conditions.

29.7 Asymptotic ω Behavior

Examination of all the Feigenbaum/bifurcation diagrams produced so far for the Duffing oscillator shows that their behavior is consistent with the hypothesis

$$\lim_{\omega \rightarrow 0} q_\infty = 0, \quad \lim_{\omega \rightarrow 0} p_\infty = 0, \quad (29.7.1)$$

$$\lim_{\omega \rightarrow \infty} q_\infty = 0, \quad \lim_{\omega \rightarrow \infty} p_\infty = 0. \quad (29.7.2)$$

That is, in the limits $\omega \rightarrow 0$ or ∞ , there is a single attracting fixed point and its basin is the entire q , p plane. Correspondingly, for each value of ϵ (and β) there is only a finite range of ω values that is of interest. In the case of Figures 5.2 and 5.3, for example, extension of the ω range to smaller and larger values shows that the advertised small and large ω asymptotic behavior has already set in so that no new features appear beyond those already seen.

To explore the $\omega \rightarrow 0$ limit, rewrite (1.1) in the form

$$q + q^3 = -\epsilon \sin \omega \tau - [\ddot{q} + 2\beta \dot{q}]. \quad (29.7.3)$$

If ω is small, we may expect that $q(\tau)$ will be slowly varying and therefore \dot{q} and \ddot{q} will be small. As an illustration of this expectation, Figure 7.1 displays the quantity $[\ddot{q} + 2\beta \dot{q}]$ as a function of τ for the periodic solution when $\omega = .01$ (and $\beta = .1$ and $\epsilon = 5.5$), the ω value associated with the left end of Figure 5.2. Note that this quantity is small, and numerical calculations verify that asymptotically it goes to zero linearly in ω as ω goes to zero.⁸ If this

⁸We remark that the ‘wiggles’ (ringing) in Figure 7.1 are real. They also appear in $q(\tau)$. If Duffing’s equation is linearized around the Ansatz (7.4), then $[\ddot{q} + 2\beta \dot{q}]$ appears as a driving term of the linearized equation. The wiggles are the (damped) response to the sharp peaks in the driving term. Examination of Figure 7.1 reveals that the wiggles occur just to the right of the peaks at $\tau = 0$ and $\tau \simeq 300$.

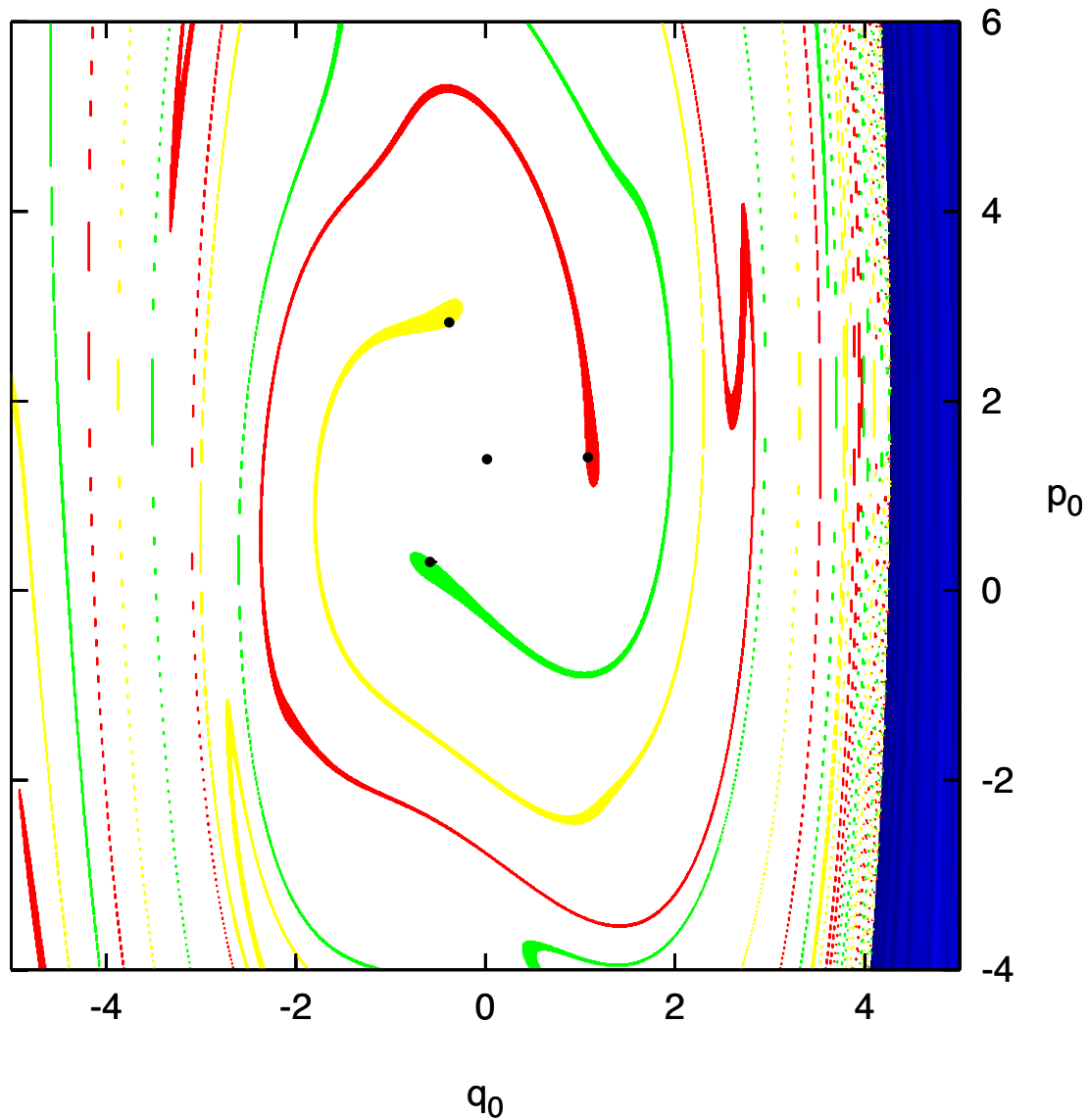


Figure 29.6.6: An enlargement of a portion of Figure 6.5. The fixed points w^1 and z^1 , z^2 , and z^3 themselves are shown as small black dots. The small black dot at the center of the figure is the fixed point w^1 . Three small black dots near the ends of the red, green, and yellow filaments surround w^1 . These are the \mathcal{M}^3 fixed points z^1 , z^2 , and z^3 , respectively. The principal components of the period-three basins contain the fixed points z^1 , z^2 , and z^3 . Note the crowding of the red, green, and yellow pieces of the period-three basins against the blue basin of w^2 (but still separated by ever smaller white areas) thereby making this basin boundary structure fractal.

quantity is neglected on the right side of (7.3), this relation becomes

$$q + q^3 = -\epsilon \sin \omega \tau \quad (29.7.4)$$

and consequently there is the result

$$q(0) + [q(0)]^3 = 0 \quad (29.7.5)$$

with the solution

$$q(0) = q_\infty = 0. \quad (29.7.6)$$

Moreover, if (7.4) holds, then there is also the relation

$$\dot{q} + 3q^2 \dot{q} = -\omega \epsilon \cos \omega \tau, \quad (29.7.7)$$

from which, using (7.6), it follows that

$$\dot{q}(0) = -\omega \epsilon. \quad (29.7.8)$$

From (7.8), in turn, we infer that

$$\lim_{\omega \rightarrow 0} \dot{q}(0) = \lim_{\omega \rightarrow 0} p_\infty = 0. \quad (29.7.9)$$

Thus, (7.1) is correct.

To explore the $\omega \rightarrow \infty$ limit, rewrite (1.1) in the form

$$\ddot{q} = -\epsilon \sin \omega \tau - [2\beta \dot{q} + q + q^3]. \quad (29.7.10)$$

If ω is very large, we may expect that $q(\tau)$ will be rapidly varying and therefore \ddot{q} will be very large compared to the other terms on the left side of (1.1). Correspondingly, the other terms will be small in the large ω limit. As an illustration of this expectation, Figure 7.2 displays the quantity $[2\beta \dot{q} + q + q^3]$ as a function of τ for the periodic solution when $\omega = 15$ (and $\beta = .1$ and $\epsilon = 5.5$), an ω value beyond the right end of Figure 5.2. We see that this quantity is indeed small, and further numerical work reveals that it vanishes as ω goes to infinity. If this quantity is neglected on the right side of (7.10), this relation becomes

$$\ddot{q} = -\epsilon \sin \omega \tau \quad (29.7.11)$$

with the solution

$$\dot{q}(\tau) = (1/\omega)\epsilon \cos \omega \tau, \quad (29.7.12)$$

$$q(\tau) = (1/\omega^2)\epsilon \sin \omega \tau. \quad (29.7.13)$$

From (7.13) we conclude that

$$\lim_{\omega \rightarrow \infty} q_\infty = \lim_{\omega \rightarrow \infty} q(0) = 0. \quad (29.7.14)$$

And from (7.12) we conclude that

$$\lim_{\omega \rightarrow \infty} p_\infty = \lim_{\omega \rightarrow \infty} \dot{q}(0) = 0. \quad (29.7.15)$$

We see that (7.2) also holds.

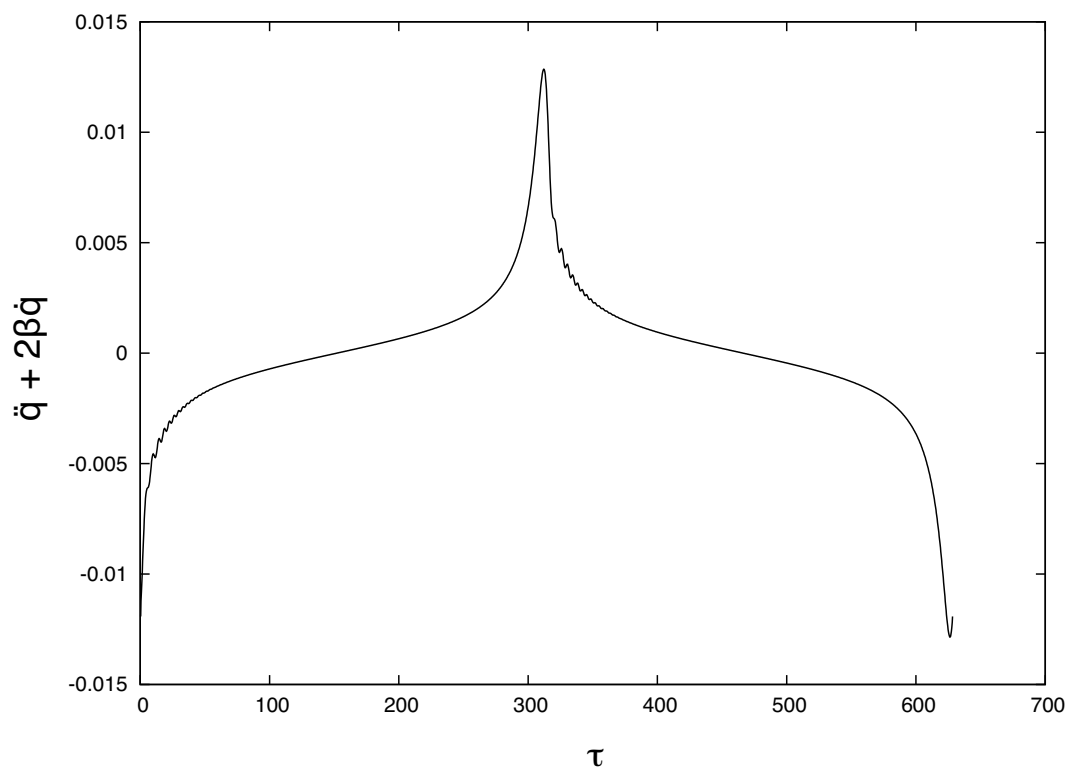


Figure 29.7.1: The quantity $[\ddot{q} + 2\beta\dot{q}]$ as a function of τ for the periodic solution when $\omega = .01$ (and $\beta = .1$ and $\epsilon = 5.5$).

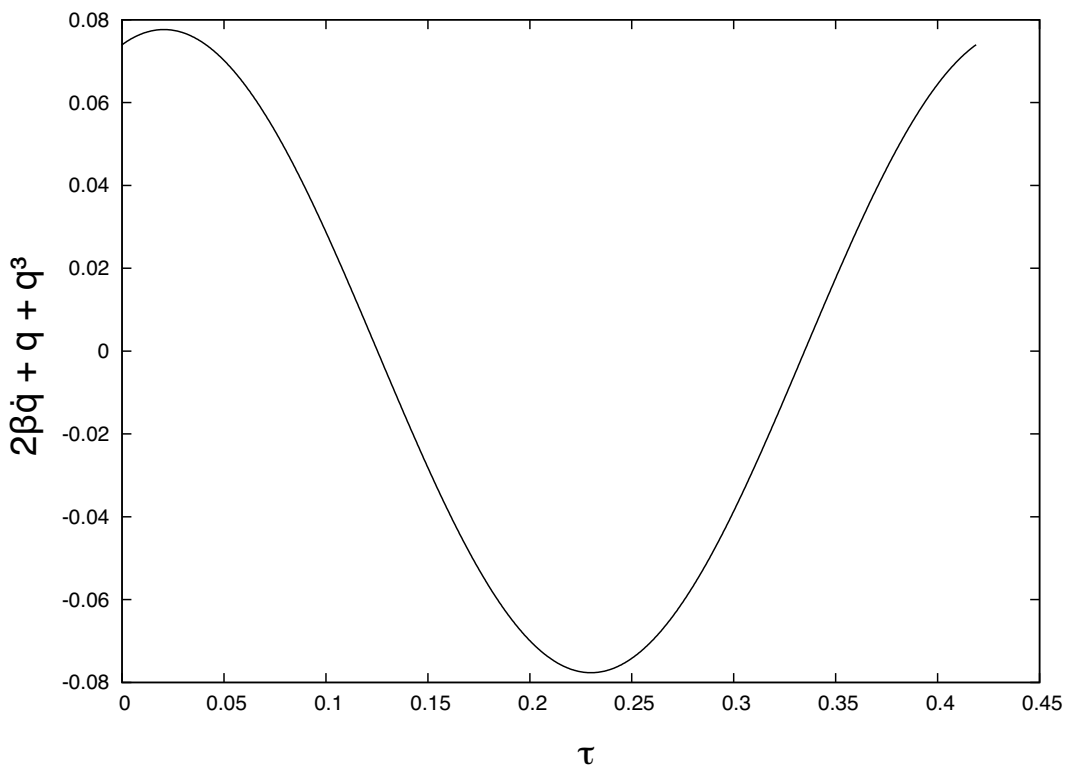


Figure 29.7.2: The quantity $[2\beta\dot{q} + q + q^3]$ as a function of τ for the periodic solution when $\omega = 15$ (and $\beta = .1$ and $\epsilon = 5.5$).

29.8 Period Doubling Cascade

We end our study of the Duffing equation by increasing ϵ from its earlier value $\epsilon = 5.5$ to larger values. Based on our experience so far, we might anticipate that the Feigenbaum diagram would become ever more complicated. That is indeed the case. Figure 8.1 displays q_∞ obtained numerically, when $\beta = 0.1$ and $\epsilon = 22.125$, as a function of ω for the range $\omega \in (0, 12)$. Evidently the behavior of the attractors for the stroboscopic Duffing map, which is what is shown in Figure 8.1, is extremely complicated. There are now a great many fixed points of \mathcal{M} itself and various powers of \mathcal{M} . For small values of ω , and as in Figures 4.1, 5.1, and 5.2, there are many resonant peaks and numerous saddle-node and pitchfork bifurcations. For larger values of ω there are more complicated bifurcations. In this figure, and some subsequent figures, the coloring scheme is chosen to guide the eye in following bifurcation trees with colors changing when the period changes. Points with period one are colored red, and points of very high or no discernible period are colored black.

Let us begin by describing the more mundane features of the diagram. As already mentioned, at the left end of the diagram there is a series of saddle-node bifurcations as before, and the first one has moved to larger ω values so that it now occurs over the range $\omega \in (4, 10)$. Also, now more numerous, there are again bubbles for small values of ω . And the first bubble has also moved to larger ω values so that it now ends near $\omega = 2$. For the right end of the diagram, numerical study indicates that there are no new structures beyond $\omega = 12$ so that the asymptotic behavior (7.14) and (7.15) sets in for ω values larger than those shown.

There are also many new features. First, there are numerous higher-period fixed points that appear and disappear through blue-sky bifurcations. Some of them have been color coded in the figure. Moreover, some of the trails of the higher-period fixed points have little bubbles, and some of these little bubbles have an infinite number of sub-bubbles within them. That is, some of the higher-period fixed points (most evidently, those of period three) seem to have complete period doubling cascades with chaotic behavior at the end of the cascade. Figure 8.2 shows this behavior in further detail. It is too complicated to be studied further here.

What we do wish to note in Figure 8.2 is that what we have been calling the the first and second bubbles have within them the *beginnings* of period doubling cascades. Recall that each of these bubbles consists of three period-one fixed points. One of them is unstable, and hence invisible in a Feigenbaum diagram. The other two are stable, and their trails as ω is varied form the bubble. We see that these cascades *do not complete* but rather, after several period doublings, each cascade ceases and then successively undoes itself by a sequence of mergers to ultimately result in what is again a single stable period-one fixed point. This behavior is similar to that exhibited by the simple map described in Appendix J.

Suppose the value of ϵ is increased still further. Figure 8.3 shows the Feigenbaum diagram when $\epsilon = 25$. It looks similar to Figure 8.1 for $\epsilon = 22.125$. For example, there are again no new structures beyond $\omega = 12$ so that the asymptotic behavior (7.14) and (7.15) sets in for ω values larger than those shown. However, Figure 8.4, which is an enlargement of Figure 8.3, shows that the Feigenbaum cascades in the first and second bubbles now go to

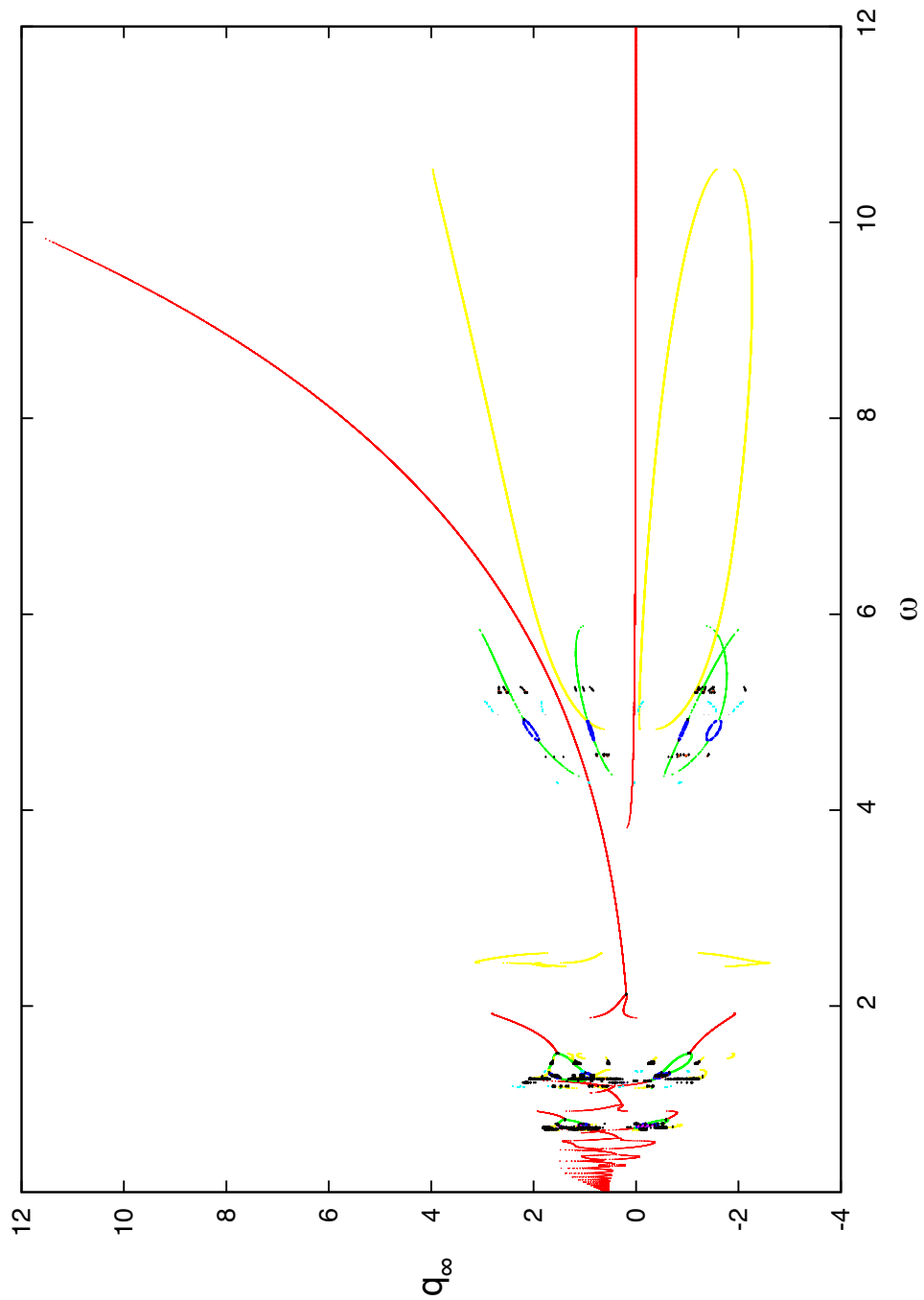


Figure 29.8.1: Feigenbaum diagram showing limiting values q_∞ as a function of ω (when $\beta = 0.1$ and $\epsilon = 22.125$) for the stroboscopic Duffing map.

completion.⁹ Then, as ω is further increased, each complete period-doubling cascade again undoes itself. Note also that there appears to be a window of stability (near $\omega = 1.33$) within the completed cascade in the first bubble.

We close this lengthy discussion with a further brief study of some aspects of the period doubling cascade in the first bubble. Figure 8.5 shows an enlargement of part of this cascade. Specifically, it shows the beginnings of the period doubling cascades that occur in the bubble. The bubble has already formed due to the pitchfork bifurcation at the value $\omega \simeq 1.2284$, a value somewhat smaller than the ω values shown, and for which $(q_\infty, p_\infty) \simeq (.3982, 2.332)$. See Figure 8.4. Within the bubble there are two period-doubling cascades that begin when $\omega \simeq 1.268$: a lower one for which $(q_\infty, p_\infty) \simeq (-.228, 1.802)$, and an upper one for which $(q_\infty, p_\infty) \simeq (1.131, 2.215)$. It can be shown that the period-doubling cascades begin at the same ω values in both the upper and lower trails because of equivariance symmetry. See Sections 29.12.2 and 29.12.3. Unfortunately the view of the upper period-doubling bifurcation is somewhat complicated by the simultaneous appearance of a wisp of the trail of the stable stable fixed point associated with the second saddle-node bifurcation (the one mostly to the left of the first bubble) that appears to overlay the period-doubling bifurcation. This is an accident of our plotting scheme that happens to occur when $\epsilon = 25$. It would not overlay the period-doubling bifurcation if we had made a Feigenbaum diagram showing p_∞ versus ω instead of q_∞ versus ω . It also does not overlay the period-doubling bifurcation for other values of ϵ . Examine Figure 8.2 (for which $\epsilon = 22.125$) in the vicinity $\omega \approx 1.22$ and $q_\infty \approx 1.2$.

Let us now examine in more detail the period-doubling cascade that occurs in the upper part of the first bubble. See Figure 8.6. Evidently, for the smaller driving frequencies and in this region of phase space, there is a single period-one fixed point corresponding to an attractor. As the frequency is increased there is an infinite cascade of period doublings, and the motion appears chaotic by $\omega \simeq 1.29$. The resemblance between Figure 8.6 and Figure 1.2.4 for the logistic map is quite striking. In particular, numerical studies indicate that the frequencies ω_j at which successive bifurcations occur behave in a way analogous to (1.2.14) with (to within numerical accuracy) Feigenbaum's value of δ . Of course, as Figure 8.3 illustrates, the Duffing stroboscopic map is vastly more complicated than the logistic map, and its behavior resembles that of the logistic map only in a limited parameter range and only in a limited region of phase space. Note also that the logistic map acts on a one-dimensional space while the Duffing stroboscopic map acts on a two-dimensional space. Figure 1.2.4 tells the full story for the logistic map. By contrast, Figure 8.6 for the Duffing stroboscopic map is a projection onto the q axis of points in the two-dimensional q, p space. For full information one would need a figure made in the style of Figures 3.2 and 5.3.¹⁰

⁹Further numerical study indicates that the cascade in the first bubble is complete by the time $\epsilon = 22.25$ while that in the second bubble remains incomplete. Shortly thereafter the cascade in the second bubble also completes. Finally, numerical study reveals that the cascades associated with the higher-period blue-sky fixed points do complete for some ϵ values less than 22.125.

¹⁰See Figure 29.7.5 for such a figure in the case of the damped Hénon map.

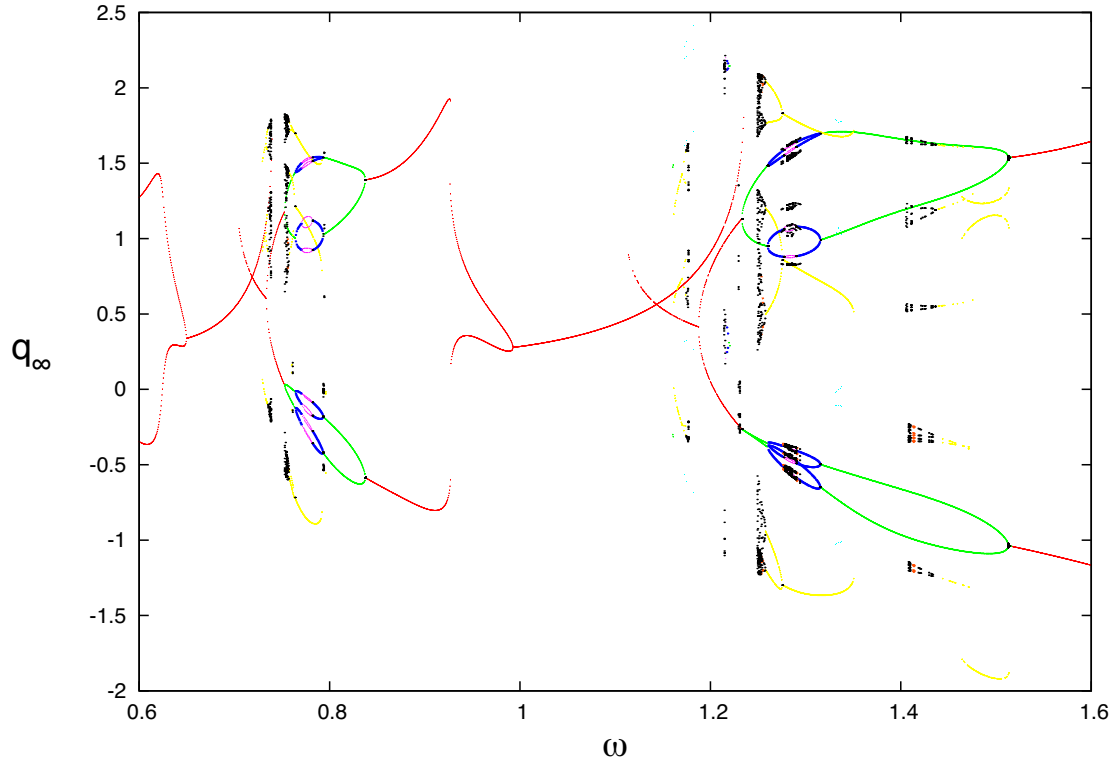


Figure 29.8.2: Enlargement of a portion of Figure 8.1 displaying limiting values of q_∞ as a function of ω (when $\beta = 0.1$ and $\epsilon = 22.125$) for the stroboscopic Duffing map. It shows part of the first bubble at the far right, the second bubble, and part of a third bubble at the far left. Examine the first and second bubbles. Each initially consists of two stable period-one fixed points. Each also contains the beginnings of period-doubling cascades. These cascades do not complete, but rather cease and then undo themselves by successive mergings to again result in a pair of stable period-one fixed points. There are also many higher-period fixed points and their associated cascades.

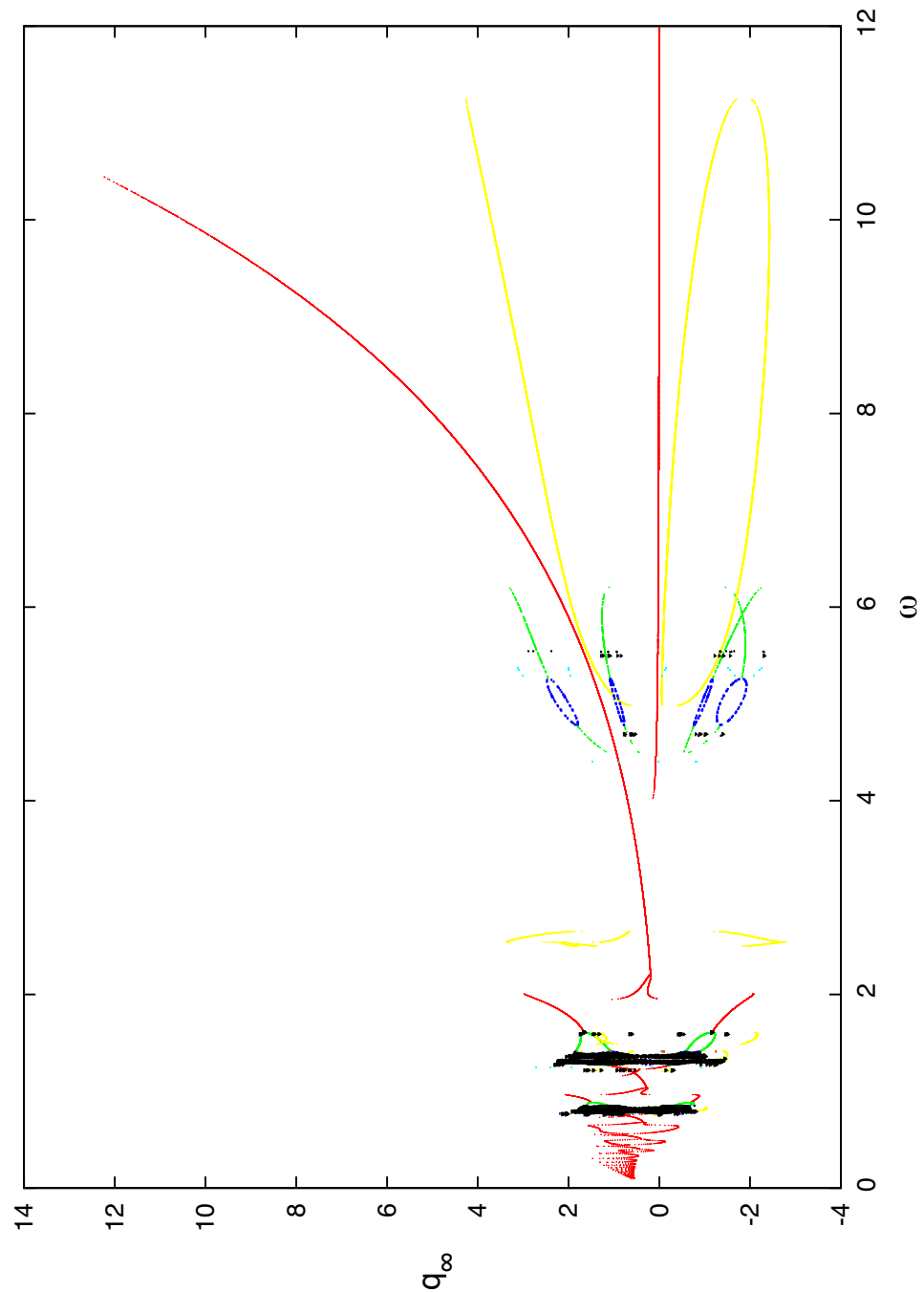


Figure 29.8.3: Feigenbaum diagram showing limiting values q_∞ as a function of ω (when $\beta = 0.1$ and $\epsilon = 25$) for the stroboscopic Duffing map.

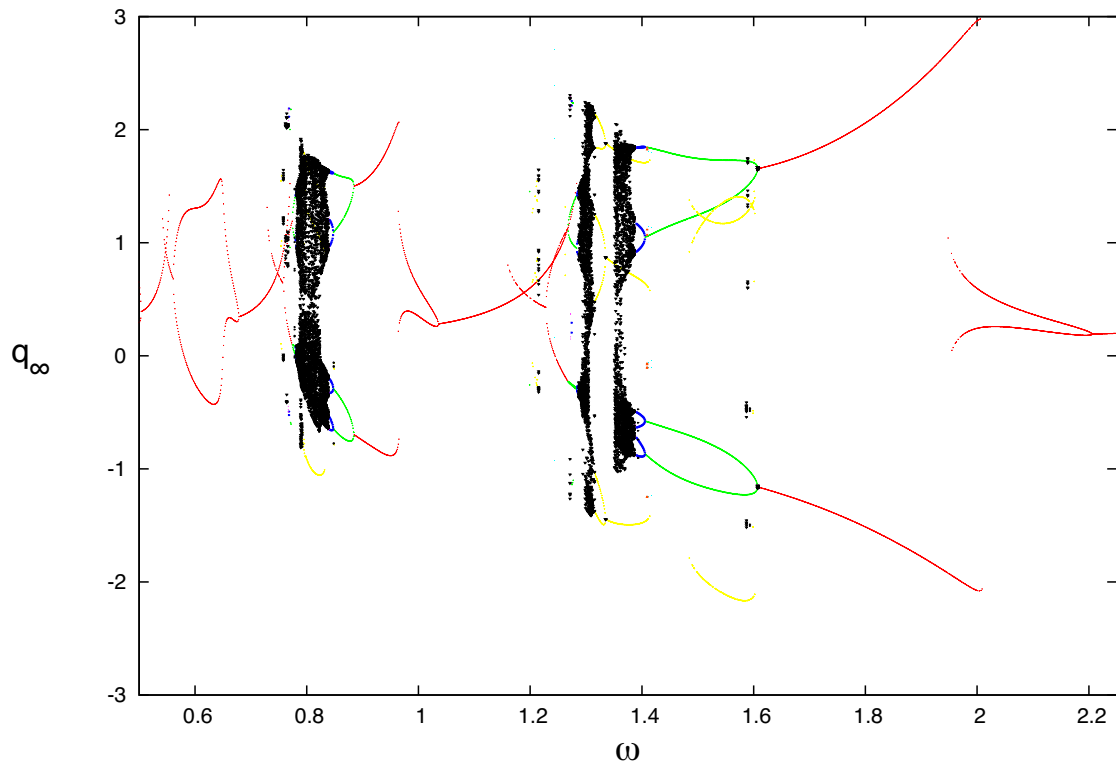


Figure 29.8.4: Enlargement of a portion Figure 8.3 showing the first, second, and third bubbles. The period-doubling cascades in each of the first and second bubbles now complete. Then they undo themselves as ω is further increased. There is no period doubling in the third bubble when $\epsilon = 25$.

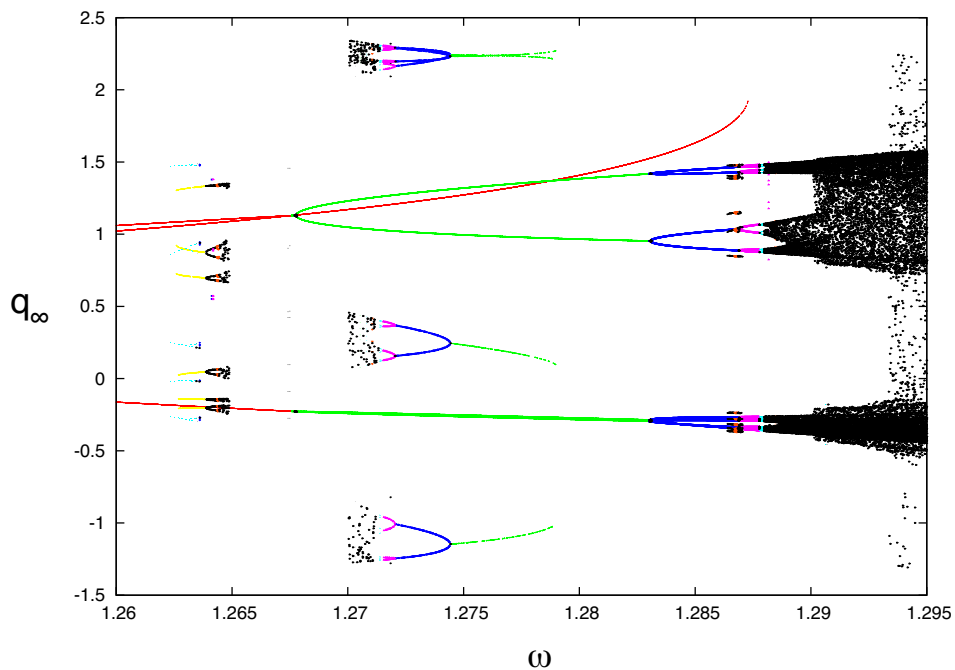


Figure 29.8.5: Detail of part of the first bubble in Figure 8.4 showing upper and lower infinite period-doubling cascades. Part of the trail of the stable fixed point associated with the second saddle-node bifurcation accidentally appears to overlay the upper period doubling bifurcation. Finally, associated with higher-period fixed points, there are numerous cascades and followed by successive mergings.

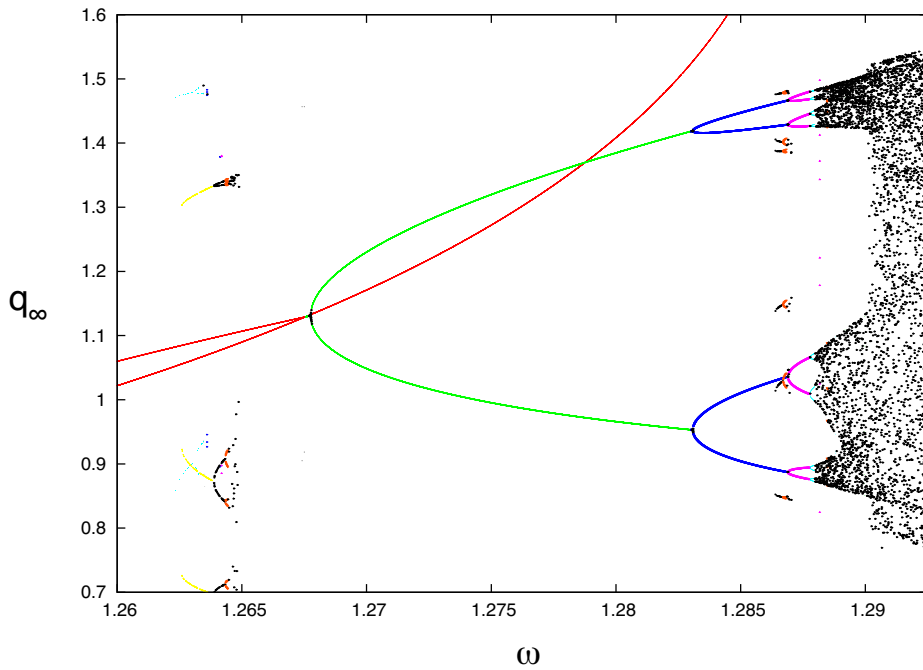


Figure 29.8.6: Detail of part of the upper cascade in Figure 8.5 showing an infinite period-doubling cascade, followed by chaos, for what was initially a stable period-one fixed point.

29.9 Strange Attractor

Finally, Figure 9.1 shows both the q_∞ and p_∞ values associated with Figure 8.6 when $\omega = 1.2902$ (and $\beta = .1$ and $\epsilon = 25$). Evidently the set of points q_∞, p_∞ for ω values just beyond the end of the cascade is quite complicated. By construction the set is an *attractor*. That is, points nearby this set are brought ever closer to the set under repeated action of \mathcal{M} . Moreover, numerical evidence suggests that this set has an infinite number of points and that the action of \mathcal{M} on points in this set is to move them about within the set in a very complicated way. Finally, the set appears to be fractal. That is, it displays self similarity under repeated magnification. Therefore it may be an instance of what is called a *strange attractor*. For example, Figure 9.2 shows an enlargement of part of Figure 9.1. Repeated enlargement is expected to show a continued self-similar structure. For an instance of a strange attractor in the case of the damped Hénon map, see Sections 29.7 and 29.9. For more about the Duffing stroboscopic map, see Section 29.12. Finally, we warn the reader that there is no universal agreement among authors about the meaning of the adjective *strange* when applied to attractors. Some simply mean that the attractor has an infinite number of points. Some take fractal behavior to be the defining feature of what it means to be strange. Others require a sensitive dependence on initial conditions. Still others require what is technically called nonuniformly hyperbolic behavior.

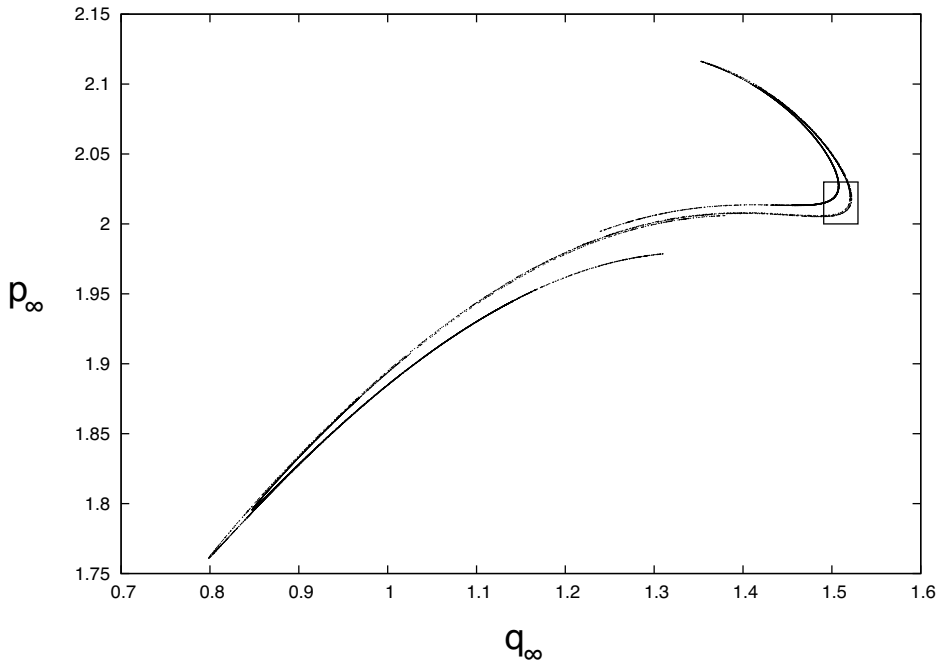


Figure 29.9.1: Limiting values of q_∞, p_∞ for the stroboscopic Duffing map when $\omega = 1.2902$ (and $\beta = .1$ and $\epsilon = 25$). They appear to lie on a strange attractor.

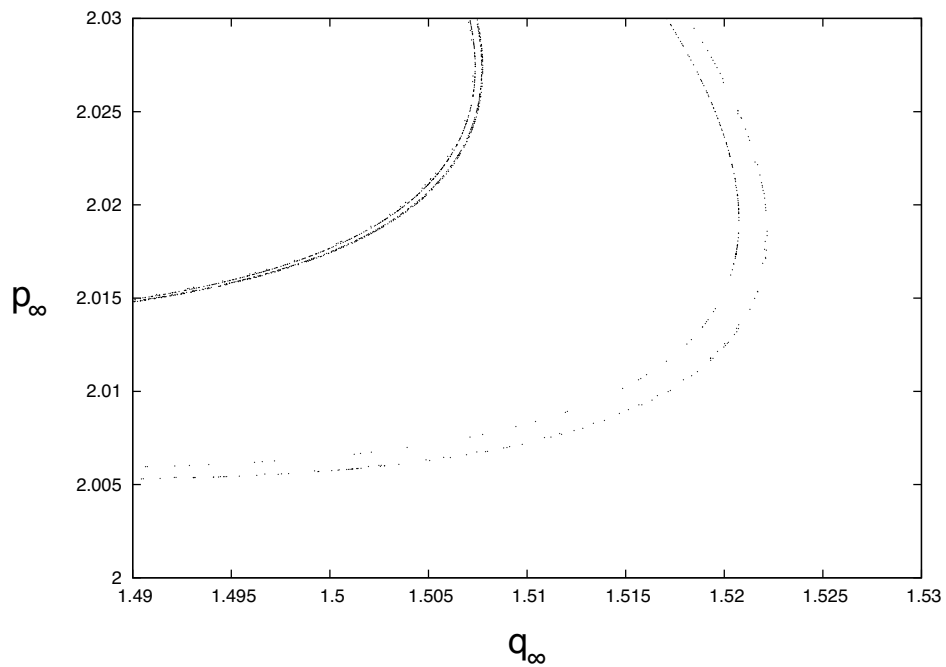


Figure 29.9.2: Enlargement of boxed portion of Figure 9.1 illustrating the beginning of self-similar fractal structure.

29.10 Acknowledgment

Dobrin Kaltchev made major contributions to the work of this chapter.

Bibliography

- [1] G. Duffing, *Erzwungene Schwingungen bei veränderlicher Eigenfrequenz und ihre technische Bedeutung*, Braunschweig, Druck und Verlag von Friedr. Vieweg und Sohn (1918).
- [2] I. Kovacic and M. Brennan, Edit., *The Duffing Equation: Nonlinear Oscillators and their Behaviour*, Wiley (2011).
- [3] V. Barger and M. Olsson, *Classical Mechanics: A Modern Perspective*, Second Edition, McGraw Hill (1995). Some of our figures and some of our discussion of Duffing's equation were motivated by Sections 11.1 through 11.4 of this book. However, we found somewhat different numerical results. Presumably this is because, for the parameter values of interest, the long-term integration of Duffing's equation requires unusual care. For our calculations we used a 10th order Adams integrator started with 6th order Runge Kutta. Integrations were performed for several different step sizes in both double and quadruple (64 and 128 bit) precision to assure satisfactory convergence. See Chapter 2.
- [4] C. Olson and M. Olsson, "Dynamical symmetry breaking and chaos in Duffing's equation", *Am. J. Phys.* **59**, p. 907 (1991).
- [5] U. Parlitz and W. Lauterborn, "Superstructure in the bifurcation set of the Duffing equation", *Physics Letters* **107A**, p. 351 (1985).
- [6] K. Becker and R. Seydel, "A Duffing equation with more than 20 branch points", *Lecture Notes in Mathematics* **878**, p. 98, E. Allgower et al., edit., Springer-Verlag (1981).
- [7] I. Kyprianidis, "Dynamics of a nonlinear electrical oscillator described by Duffing's equation", Aristotle University of Thessaloniki (Greece) Physics Department Report, apparently unpublished but available on the Web.
- [8] J. M. T. Thompson and H. B. Stewart, *Nonlinear Dynamics and Chaos*, Second Edition, John Wiley (2002).
- [9] R. Van Dooren and M. De Groote, "Numerical Evidence of Feigenbaum's δ in Nonlinear Oscillations", *Journal of Computational Physics* **105**, 173-177 (1993).
- [10] J. Guckenheimer and P. Holmes, *Nonlinear Oscillations, Dynamical Systems, and Bifurcations of Vector Fields*, Springer-Verlag (1990).

- [11] D. Jordan and P. Smith, *Nonlinear Ordinary Differential Equations*, Oxford University Press (1979).
- [12] D. Ruelle, “What Is a Strange Attractor?”, *Notices of the American Mathematical Society* **53**, p. 764, August 2006.
- [13] Duffing equation Web sites. Any search engine will find several Web sites devoted to the Duffing equation.